5064–5079 *Nucleic Acids Research, 2022, Vol. 50, No. 9* *Published online 7 May 2022*
https://doi.org/10.1093/nar/gkac316

APIP5 functions as a transcription factor and an RNA-binding protein to modulate cell death and immunity in rice

Fan Zhang [1], Hong Fang[1], Min Wang[1], Feng He[1], Hui Tao[1], Ruyi Wang[1], Jiawei Long[1], Jiyang Wang[1], Guo-Liang Wang [2,*] and Yuese Ning [1,*]

[1]State Key Laboratory for Biology of Plant Diseases and Insect Pests, Institute of Plant Protection, Chinese Academy of Agricultural Sciences, Beijing 100193, China and [2]Department of Plant Pathology, The Ohio State University, Columbus, OH 43210, USA

Received December 30, 2021; Revised April 08, 2022; Editorial Decision April 19, 2022; Accepted April 20, 2022

ABSTRACT

Many transcription factors (TFs) in animals bind to both DNA and mRNA, regulating transcription and mRNA turnover. However, whether plant TFs function at both the transcriptional and post-transcriptional levels remains unknown. The rice (*Oryza sativa*) bZIP TF AVRPIZ-T-INTERACTING PROTEIN 5 (APIP5) negatively regulates programmed cell death and blast resistance and is targeted by the effector AvrPiz-t of the blast fungus *Magnaporthe oryzae*. We demonstrate that the nuclear localization signal of APIP5 is essential for APIP5-mediated suppression of cell death and blast resistance. APIP5 directly targets two genes that positively regulate blast resistance: the cell wall-associated kinase gene *OsWAK5* and the cytochrome P450 gene *CYP72A1*. APIP5 inhibits *OsWAK5* expression and thus limits lignin accumulation; moreover, APIP5 inhibits *CYP72A1* expression and thus limits reactive oxygen species production and defense compounds accumulation. Remarkably, APIP5 acts as an RNA-binding protein to regulate mRNA turnover of the cell death- and defense-related genes *OsLSD1* and *OsRac1*. Therefore, APIP5 plays dual roles, acting as TF to regulate gene expression in the nucleus and as an RNA-binding protein to regulate mRNA turnover in the cytoplasm, a previously unidentified regulatory mechanism of plant TFs at the transcriptional and post-transcriptional levels.

INTRODUCTION

Programmed cell death (PCD) is a ubiquitous genetically regulated process in prokaryotes and eukaryotes. In plants, PCD occurs during germination, growth, development and senescence, or under abiotic or biotic stresses (1). For example, PCD has important functions in disease resistance: the hypersensitive response (HR), a plant-specific form of PCD, occurs during effector-triggered immunity (ETI) (2) and pathogen-associated molecular pattern (PAMP)-triggered immunity (PTI) (3,4). The PCD and plant immunity pathways are intertwined and defense signal transduction cascades depend on several layers of gene regulation at the transcriptional, translational and post-translational levels (5,6).

Transcription factors (TFs) play pivotal roles in regulating the transcriptional reprograming of plant immune responses and the coordination of defense signaling networks with other stress and growth pathways (7). Most TFs localize to the nucleus where they bind to DNA and selectively activate or suppress defense gene expression (7). The cytoplasmic-nuclear trafficking of activated TFs is also essential for their specific roles in different cellular compartments (8,9). For example, the NAC TFs NAC Targeted by *Phytophthora* (NTP) 1 and NTP2 were released from the endoplasmic reticulum membrane into the nucleus in potato (*Solanum tuberosum*) following treatment with *P. infestans* culture filtrate, while the RXLR effector Pi03192 directly interacted with and inhibited their re-localization to prevent defense activation (10). Similarly, the membrane-tethered NAC TF BnaNAC60 from oilseed rape (*Brassica napus*) was translocated into the nucleus in response to oxidative stress, inducing reactive oxygen species (ROS) accumulation and HR-like cell death, in transgenic tobacco (*Nicotiana tabacum*) (11).

Some TFs are re-translocated into the cytoplasm to regulate PCD or other cellular processes during pathogen infection. For example, when the basic leucine zipper (bZIP) TF bZIP10 was co-expressed with its interactor LESIONS SIMULATING DISEASE 1 (LSD1) in *Arabidopsis thaliana*, its binding activity was weakened and most of the bZIP10 was translocated into the cyto-

*To whom correspondence should be addressed. Tel: + 86 10 62817045; Fax: +86 10 62817045; Email: ningyuese@caas.cn
Correspondence may also be addressed to Guo-Liang Wang. Tel: +1 614 292 9280; Fax: +1 614 292 4455; Email: wang.620@osu.edu

plasm, thereby enhancing LSD1-mediated cell death and antagonistically modulating RECOGNITION OF PERONOSPORA PARASITICA 2 (RPP2)-mediated resistance to *Hyaloperonospora parasitica* (12). However, the molecular mechanisms underlying the dynamic homeostasis of TFs in different subcellular compartments in PCD and plant immunity, and the effects of changes in TF localization, are largely unknown.

The bZIP TF family is one of the largest TF families in plants. Most bZIP TFs investigated to date localize to the nucleus, preferentially bind to *cis* elements with an ACGT core sequence in their target genes via their basic region, and form dimers via their the leucine zipper region (13). In *Arabidopsis*, several bZIP TFs are known to be involved in plant immunity such as the TGACG-Binding (TGA) subfamily members in NON-EXPRESSOR OF PATHOGENESIS-RELATED GENES 1 (NPR1)-mediated resistance (14) and ELONGATED HYPOCOTYL 5 (HY5) in ENHANCED DISEASE SUSCEPTIBILITY 1 (EDS1)-dependent ROS and salicylic acid signaling (15) and defense to *Hyaloperonospora arabidopsidis* (16). Among the 89 bZIP TFs in rice (*Oryza sativa*), several are known to regulate PCD and plant immunity, but the target genes of only a few TFs have been identified. For instance, rTGA2.1/OsbZIP63 coordinates with rice NPR1 HOMOLOG 1 (NH1) to activate the expression of *CYSTEINE RECEPTOR KINASE 6* (*CRK6*) and *CRK10* during NH1-mediated immunity against *Xanthomonas oryzae* pv. *oryzae* (*Xoo*) (17). OsTGA2/OsbZIP28 selectively binds to TGACGT sequences in the promoters of defense-related genes and overexpressing *OsTGA2/OsbZIP28* significantly increased resistance to *Xoo* (18).

In animal systems, a significant number of TFs bind to mRNAs to regulate their turnover (19,20). These DNA and RNA binding proteins allow multiple signals to be integrated into cellular signaling networks for the fine-tuning of target gene expression and the modulation of cellular metabolism during stress. To date, no plant TF has been shown to bind to mRNA to regulate target gene expression at the post-transcriptional level. Nevertheless, a few RNA-binding proteins exhibit DNA-binding activity in plants. For example, the tandem zinc finger domain-containing CCCH proteins TZF1, C3H14 and C3H15 in *Arabidopsis* show both RNA- and DNA-binding capacity and shuttle between cytoplasmic foci and the nucleus (21–23). In rice, the CCCH-type zinc finger protein OsLIC binds to both double-stranded DNA and single-stranded poly(A), (G) and (U) (24). However, the target genes of these CCCH proteins remain to be identified. Another example is the RNA recognition motif (RRM)-containing protein PIBP1 in rice, which not only has RNA-binding capacity but can also bind to the *OsWAK14* and *OsPAL1* promoters to modulate resistance to *Magnaporthe oryzae* (25).

We previously demonstrated that the rice bZIP TF AVRPIZ-T-INTERACTING PROTEIN 5 (APIP5) negatively regulates PCD and immunity against *M. oryzae*, and is directly suppressed by the *M. oryzae* effector AvrPiz-t (26). APIP5 contains a nuclear localization signal (NLS) motif and a nuclear export signal (NES) motif and mainly localizes to the cytoplasm. In the current study, we discovered that the NLS of APIP5 is essential for APIP5-mediated repression of age-dependent cell death and resistance to *M. oryzae*. Upon pathogen infection, APIP5 translocates from the cytoplasm to the nucleus and directly suppresses the expression of the defense-related genes *WALL ASSOCIATED KINASE 5* (*OsWAK5*) and *CYTOCHROME P450 72A1* (*CYP72A1*), thereby weakening lignin and ROS accumulation. Intriguingly, APIP5 also functions as an unconventional RNA-binding protein that directly targets and regulates the mRNA turnover of the cell death- and defense-related genes *OsLSD1* (a functional homolog of *LSD1* in *Arabidopsis*) and *RHO-LIKE GTPASE GENE 1* (*OsRac1*) to regulate PCD and plant immunity against *M. oryzae*. Therefore, APIP5 plays dual roles as a TF and an RNA-binding protein in cell death and defense pathways.

MATERIALS AND METHODS

Plant materials and growth conditions

All transgenic rice lines used in this study are in the Nipponbare (NPB) background. Rice plants were grown in a greenhouse for breeding and phenotypic observation. Plants used for *M. oryzae* inoculation were grown in growth chambers (26/20°C day/night, 70% humidity with a 12-h light/dark photoperiod). *Nicotiana benthamiana* plants used for transient expression were grown in a phytotron at 22°C under a 16-h light/8-h dark photoperiod.

Blast fungus inoculation and disease resistance assay

Magnaporthe oryzae isolate was cultured on oatmeal medium in the dark for 7 days at 26°C and transferred to the light for sporulation for 7–10 days before use. The spore concentration in the suspension was adjusted to approximately 5×10^5 conidia/ml for punch inoculation. Six-week-old rice plants were subjected to punch inoculation as previously described (27). At 14 days after inoculation, the inoculated leaves were photographed, and relative fungal biomass was determined by DNA-based quantitative PCR as previously reported (27). All inoculation experiments were repeated at least three times independently. The primers used for PCR analysis are listed in Supplementary Table S1.

Nuclear and cytoplasmic protein extraction

Cell fractionation assays were performed as described previously (28). Briefly, 0.5 g samples of *GFP-APIP5* and *GFP-APIP5nls* plants were homogenized in liquid nitrogen and mixed with Honda buffer (25 mM Tris-HCl, pH 7.4, 10 mM $MgCl_2$, 0.4 M sucrose, 2.5% Ficoll 400, 5% dextran, 10 mM β-mercaptoethanol, 1 mM phenylmethylsulfonyl fluoride [PMSF], 0.5% Triton X-100 with 5 mM DTT and 1 × protease inhibitor cocktail [Roche, Cat. No. 04693132001] added before use). Each mixture was vortexed, incubated on ice for 30 min and filtered through Miracloth (Millipore, 475855). The flow-through was centrifuged at 1500 *g* for 5 min at 4°C, and the supernatants were collected as the cytoplasmic fraction. The pellets were washed with Honda buffer, centrifuged at 1000 *g* for 5 min at 4°C to pellet starch and cellular debris, and re-centrifuged at 1800 *g* for 5 min at

4°C to pellet the nuclei. The pellets were washed eight times with nuclear re-suspension buffer (20 mM Tris-HCl, pH 7.5, 2.5 mM $MgCl_2$, 25% glycerol, 0.2% Triton X-100, 5 mM β-mercaptoethanol and 1 mM PMSF, with 1 × protease inhibitor cocktail [Roche, Cat. No. 04693132001] added before use). The pellets were resuspended in denatured extraction buffer (50 mM Tris-HCl, pH 7.5, 150 mM NaCl, 4 M urea and 1 mM PMSF), vortexed and centrifuged at 16 000 *g* at 4°C. The supernatants were collected as the nuclear fractions. Both the cytoplasmic and nuclear fractions were mixed with 4 × SDS loading buffer and boiled for the immunoblot assays. GFP-APIP5 and GFP-APIP5nls were detected using anti-GFP antibody (Roche, Cat. No. 11814460001). HSP82 proteins were detected using anti-HSP antibody (Beijing Protein Innovation, AbM51099-31-PU) as a cytoplasmic marker, and histone H3 proteins were detected using anti-Histone H3 antibody (TransGen, HL102) as a nuclear marker.

Electrophoretic mobility shift assay (EMSA)

EMSA was performed as described previously (29). The recombinant proteins MBP, MBP-APIP5, MBP-APIP5nls and MBP-APIP5nes were expressed in *Escherichia coli* Rosetta (DE3) and purified with amylose resin (NEB, E8201) according to the manufacturer's instructions. DNA fragments were 5′-end-labeled with 5-carboxyfluorescein (FAM). The labeled DNA probes were incubated with purified MBP, MBP-APIP5, MBP-APIP5nls and MBP-APIP5nes in a 20 μl binding reaction system (50 mM Tris-HCl, pH 7.5, 5 mM EDTA, 10 mM $MgCl_2$, 0.5 M NaCl, 5 mM DTT, 0.05 mg/mL poly [dI-dC] and 40% glycerol) at 25°C for 30 min. For the competition assays, non-labeled competitor DNA probe was also added to the reaction. The reaction mixtures were electrophoresed at 4°C on a 6% native polyacrylamide gel in 0.5 × Tris-borate-EDTA (TBE) buffer for 60-90 min and imaged on a Typhoon 9400 imager (GE Healthcare).

For RNA EMSA, synthesized RNA fragments were 5′-end-labeled with FAM and incubated with MBP, MBP-APIP5, MBP-APIP5nls and MBP-APIP5nes. For the competition assay, unlabeled RNA fragments were added to the reactions. The reaction mixtures were also electrophoresed at 4°C on a 6% native polyacrylamide gel in 0.5 × TBE buffer and imaged on a Typhoon 9400 imager (GE Healthcare). EMSA experiments were repeated three times.

Dual-luciferase reporter assay

The ∼2000-bp *OsWAK5* and *CYP72A1* promoter sequences were amplified from NPB genomic DNA and inserted into *pGreenII 0800-LUC* vector through *Hind*III + *BamH*I and *Sal*I + *Sma*I to generate the reporter constructs, respectively. The Renilla luciferase (*REN*) gene under the control of the 35S promoter in the *pGreenII 0800-LUC* vector was used as the internal control, and the *35SPro::GFP*, *35SPro::GFP-APIP5nls* and *35SPro::GFP-APIP5nes* constructs were used as effectors. The plasmids were infiltrated into *N. benthamiana* leaves. At 48-70 h after infiltration, leaf discs were collected and examined for LUC activity using the Dual-Luciferase Reporter Assay System (Promega, E2920) with a GLOMAX 96 microplate luminometer (Promega).

Chromatin immunoprecipitation (ChIP) assay

The ChIP assay was performed as previously reported (30). Briefly, the precipitated DNA fragments were recovered with cetyltrimethyl ammonium bromide (CATB) and dissolved in sterile water for constructing the sequencing library. The libraries were constructed according to Illumina's instructions, and then sequenced on the Illumina Hiseq X10. The high-quality reads were mapped to the MSU Rice Genome Annotation Project database using Bowtie2 (31,32). The enriched peaks were identified using MACS (version 2.0.0) software and annotated using ChIPseeker (33,34), which was followed by MEME Suite (MEME and DREME tools for motif discovery, and TOMTOM searches for similar motifs in databases of known motifs) to generate the APIP5-binding motif (35). The raw sequence data reported in this paper were deposited in Gene Expression Omnibus (GEO), under accession number GSE198135.

For ChIP-qPCR assay, *N. benthamiana* leaves co-infiltrated with *GFP, GFP-APIP5nls* or *GFP-APIP5nes* and reporter plasmids (*0800-OsWAK5Pro* or *0800-CYP72A1Pro*) or the leaves of *GFP-APIP5*, *GFP-APIP5nls* and *GFP-APIP5nes* rice plants at the tillering stage were ground into a power in liquid nitrogen, and the extracted protein was cross-linked in cross-linking buffer with 1% (v/v) formaldehyde via vacuum infiltration for 15 min. Glycine (0.25 M) was added to quench the cross-linking reaction. The chromatin complexes were isolated, sonicated and immunoprecipitated with anti-GFP antibody (Roche, Cat. No. 11814460001). Immunoprecipitated proteins were captured by Protein G magnetic beads (Invitrogen, 88847) and thoroughly washed to remove non-specific bound DNA fragments. The precipitated and input DNA fragments were recovered with CTAB and dissolved in sterile water. ChIP-qPCR results were calculated as the percentage of input DNA. Independent ChIP-qPCR experiments were performed three times with similar results. All primers used for ChIP-qPCR are listed in Supplementary Table S1.

In vitro and *in vivo* RNA-immunoprecipitation (RIP) assays

In vitro RIP assays were performed as previously described (36). Briefly, total RNA was extracted from rice plants and divided into two equal fractions for incubation with MBP-APIP5 or MBP. MBP and MBP-APIP5 were purified with amylose resins (NEB, E8201) and washed five times with binding/washing buffer (150 mM NaCl, 20 mM Tris-HCl, pH 8.0, 2 mM EDTA, 1% Triton X-100, 0.1% SDS and 20 units/ml RNase inhibitor [Invitrogen, N8080119]). Following incubation with total RNA for 3 h at 4°C, RNA/MBP and RNA/MBP-APIP5 resin complexes were thoroughly washed eight times with binding/washing buffer and combined with TRIzol reagent (Invitrogen, 15596018) to extract RNA. The cDNA synthesized from the eluted RNA was used for qRT-PCR. Each RIP value was normalized to its respective input RNA value.

For the *in vivo* RIP assay, 2-week-old *GFP-APIP5* seedlings were homogenized in liquid nitrogen, cross-linked in cross-linking buffer with 1% (v/v) formaldehyde, and suspended in extraction buffer (100 mM KCl, 2.5 mM $MgCl_2$, 10 mM HEPES pH 7.5, 10% glycerol, 0.5% NP40, 1 mM DTT, 100 U/ml RNasin RNase inhibitor [Invitrogen, N8080119], 25 mM MG132 and EDTA-free protease inhibitor cocktail [Roche, Cat. No. 04693132001]). Following two rounds of centrifugation at 16 000 *g* for 10 min at 4°C to remove the insoluble material, the supernatants were divided into two fractions and incubated with or without anti-GFP antibodies (Roche, Cat. No. 11814460001) for 2 h at 4°C before adding Protein G magnetic beads (Invitrogen, 88847). The bead mixtures were washed ten times with washing buffer (100 mM KCl, 2.5 mM $MgCl_2$, 10 mM HEPES pH 7.5, 10% glycerol, 0.5% NP40, 40 U/ml RNasin RNase inhibitor [Invitrogen, N8080119]) and eluted with TRIzol reagent (Invitrogen, 15596018). The resulting RNA was analyzed by qRT-PCR.

Analysis of cellulose and lignin content

To analyze cellulose and lignin contents, 6- to 8-week-old *OsWAK5*-overexpression and NPB plants were harvested individually and dried thoroughly at 60°C. Dry leaf tissue (0.3 g) was ground in liquid nitrogen. The cellulose content was measured according to the method described previously (37).

To analyze lignin content, after adding 7 ml of 50 mM potassium phosphate buffer (pH 7.0), the mixtures were incubated at 4°C overnight and centrifuged at 1400 *g* for 10 min. The pellets were extracted with the following solvents: 7 ml PBS (pH 7.0; repeated twice), 7 ml PBS containing 1% (v/v) Triton X-100 (repeated three times), 7 ml PBS containing 1 M NaCl (repeated twice), 7 ml distilled water (repeated twice) and 5 ml acetone (repeated twice). The pellets were dried at 60°C for 24 h to obtain protein-free cell wall samples. The acetyl bromide method was used to quantify lignin content as described previously (38).

Measuring Cytochrome *c* Oxidase (COX) complex activity and oxidative burst

COX IV activity in *CYP72A1*-overexpression and NPB plants was measured using a Mitochondrial Complex IV Assay Kit (FHTD-2-Y, Suzhou Keming Biotechnology) according to the manufacturer's protocol.

Oxidative burst detection in *CYP72A1-OE*, *Cas9-cyp72a1* and NPB plants was detected as described previously (39).

Statistical analysis

All data for quantification analyses are presented as mean ± standard error (SE). Statistical analysis was performed by two-tailed Student's *t*-test (*$P < 0.05$, **$P < 0.01$).

Accession numbers

The accession numbers of major genes mentioned in this study are as follows: APIP5 (LOC_Os06g50310), OsWAK5 (LOC_Os01g26174), CYP72A1 (LOC_Os03g25500), OsLSD1 (LOC_Os08g06280) and OsRac1 (LOC_Os01g12900).

RESULTS

APIP5 regulation of age-dependent cell death and plant immunity requires its NLS

We previously demonstrated that APIP5 contains an NLS in its DNA-binding domain and an NES in its C terminus (26). To further explore the functions of these domains in APIP5, we mutated the hydrophilic amino acids in the NLS and NES to alanine (Ala), producing APIP5nls and APIP5nes, respectively (Supplementary Figure S1A). We then generated N-terminal green fluorescent protein (GFP)-labeled fusion proteins with APIP5, APIP5nls and APIP5nes. When the constructs encoding these proteins were expressed in rice protoplasts, GFP-APIP5 and GFP-APIP5nls primarily localized to the cytoplasm, whereas GFP-APIP5nes mainly localized to the nucleus (Supplementary Figure S1B). Meanwhile, APIP5nls and APIP5nes had similar self-transactivation activities in yeast and formed homodimers in *N. benthamiana* and rice protoplasts, like APIP5 (Supplementary Figure S1C–G). These results suggest that the mutations in the NLS and NES do not affect the self-transactivation activity or homodimerization of APIP5. Furthermore, APIP5nls formed heterodimers with APIP5 in yeast-two hybrid (Y2H), luciferase complementation (LCI), and glutathione S-transferase (GST) pull-down assays (Supplementary Figure S1H–J).

To investigate the biological functions of the APIP5 NLS and NES in APIP5-mediated cell death and blast resistance, we cloned *APIP5*, *APIP5nls* and *APIP5nes* into the transformation vector *pRHVnGFP* under the control of the maize *UBIQUITIN* promoter. The resulting plasmids containing *GFP-APIP5*, *GFP-APIP5nls* and *GFP-APIP5nes* were transformed into the *japonica* rice cultivar Nipponbare (NPB). Because the dimerization of GFP-APIP5, APIP5nls and APIP5nes with the intrinsic APIP5 may interfere with the ectopic expression of the transgenes, we checked the transcript and protein levels of GFP-APIP5, APIP5nls and APIP5nes in the transgenic plants by quantitative reverse-transcription PCR (qRT-PCR) and immunoblot analysis. The results showed that the transcript and protein levels of GFP-APIP5, APIP5nls and APIP5nes were much higher than the intrinsic APIP5 (Supplementary Figure S2A–F). We also used CRISPR/Cas9 to generate *Cas9-apip5* mutants, and *APIP5* was significantly down-regulated in the mutants than in NPB plants (Supplementary Figure S2G and H).

At the seedling stage, *GFP-APIP5*, *GFP-APIP5nls* and *GFP-APIP5nes* transgenic plants and *Cas9-apip5* mutants grew normally and accumulated similar levels of H_2O_2 compared to NPB, as detected by 3,3′-diaminobenzidine (DAB) staining (Supplementary Figure S3). However, at the tillering stage, both *GFP-APIP5nls* and *Cas9-apip5* mutant plants displayed cell death-like lesions and greater H_2O_2 accumulation on the older leaves (Figure 1A and B; Supplementary Figure S4A). However, the growth of *GFP-APIP5* and *GFP-APIP5nes* transgenic plants was similar to NPB at this stage (Supplementary Figure S4C, D, F

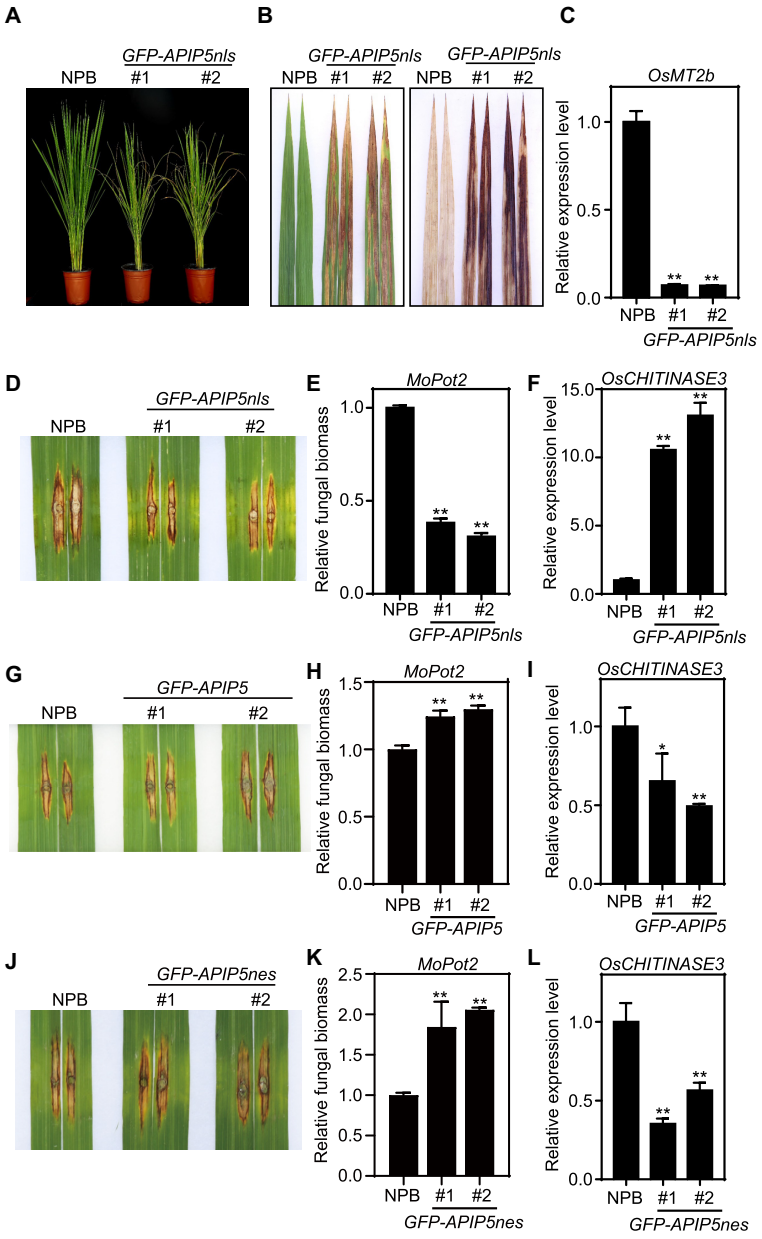

Figure 1. The nuclear localization signal is required for avoiding *APIP5*-mediated age-dependent cell death and resistance to *M. oryzae*. (**A**) Cell death phenotypes of *GFP-APIP5nls* transgenic plants growing in a greenhouse. (**B**) Cell death phenotypes in the leaves of *GFP-APIP5nls* transgenic plants (left panel) and ROS levels detected by DAB staining (right panel). (**C**) Expression levels of cell death-related gene *OsMT2b* in *GFP-APIP5nls* transgenic plants detected by qRT-PCR. *UBIQUITIN* (*UBI*) was used as an internal control. Values are means ± SE ($n = 3$, technical repeats). The mean and SE values were obtained from three biological samples (one leaf disc each). (**D** and **E**) Disease symptoms and relative fungal biomass of representative leaves of *GFP-APIP5nls* and NPB plants after punch inoculation with *M. oryzae* isolate RO1-1. The images were taken at 14 d after inoculation. Similar results were obtained from three independent experiments (biological replicates), and the representative data from one replicate are shown. Values are means ± SE ($n = 3$, technical repeats). The mean and SE values were obtained from five samples. (**F**) Expression levels of defense-related gene *OsCHITINASE3* in *GFP-APIP5nls* transgenic plants detected by qRT-PCR. *UBI* was used as an internal control. Values are means ± SE ($n = 3$, technical repeats). The mean and SE values were obtained from three biological samples (one leaf disc each). (**G** and **H**) Disease symptoms and relative fungal biomass of representative leaves of *GFP-APIP5* and NPB plants after punch inoculation with *M. oryzae* isolate RO1-1. The images were taken at 14 d after inoculation. Similar results were obtained from three independent experiments (biological replicates), and the representative data from one replicate are shown. Values are means ± SE ($n = 3$, technical repeats). The mean and SE values were obtained from five samples. (**I**) Expression levels of defense-related gene *OsCHITINASE3* in *GFP-APIP5* transgenic plants detected by qRT-PCR. *UBI* was used as an internal control. Values are means ± SE ($n = 3$, technical repeats). The mean and SE values were obtained from three biological samples (one leaf disc each). (**J** and **K**) Disease symptoms and relative fungal biomass of representative leaves of *GFP-APIP5nes* and NPB plants after punch inoculation with *M. oryzae* isolate RO1-1. The images were taken at 14 d after inoculation. Similar results were obtained from three independent experiments (biological replicates), and the representative data from one replicate are shown. Values are means ± SE ($n = 3$, technical repeats). The mean and SE values were obtained from five samples. (**L**) Expression levels of defense-related gene *OsCHITINASE3* in *GFP-APIP5nes* transgenic plants detected by qRT-PCR. *UBI* was used as an internal control. Values are means ± SE ($n = 3$, technical repeats). The mean and SE values were obtained from three biological samples (one leaf disc each). Asterisks represent significant difference determined by Student's *t*-test ($^*P < 0.05$, $^{**}P < 0.01$) compared to NPB.

and G). Consistent with this phenotype, *ORYZA SATIVA METHALLOTHIONEIN2b* (*OsMT2b*), encoding a negative regulator of cell death, was significantly downregulated in both *GFP-APIP5nls* and *Cas9-apip5* plants compared with NPB (Figure 1C and Supplementary Figure S4B). By contrast, the expression of *OsMT2b* was not discernibly affected in *GFP-APIP5* or *GFP-APIP5nes* plants (Supplementary Figure S4E and H). Additionally, to confirm GFP-APIP5 is functional, we transformed the *Cas9-apip5* construct into the calli of *GFP-APIP5* overexpression seeds and obtained transgenic plants with deletions in the endogenous *APIP5* gene and the intact *GFP-APIP5* transgene. The *Cas9-apip5*/*GFP-APIP5* transgenic plants did not show any cell death and excessive accumulation of H_2O_2, which was similar with that of NPB and *GFP-APIP5* plants (Supplementary Figure S4I and J). These results indicate that GFP-APIP5 can functionally complement *Cas9-apip5* and the NLS in APIP5 is essential for the negative regulation of age-dependent cell death in rice.

Next, we punch-inoculated *GFP-APIP5*, *GFP-APIP5nls* and *GFP-APIP5nes* plants with the compatible *M. oryzae* isolate RO1-1 before visible cell death lesions appeared on *GFP-APIP5nls* plants. Compared to NPB plants, *GFP-APIP5nls* plants exhibited elevated resistance level to RO1-1 with reduced fungal biomass (Figure 1D and E), while *GFP-APIP5* and *GFP-APIP5nes* plants displayed decreased resistance, with elevated fungal biomass (Figure 1G, H, J and K). Additionally, *GFP-APIP5* and *GFP-APIP5nes* transgenic plants were also more susceptible to both RB22 (without *AvrPiz-t*) and RB22-*AvrPiz-t* isolates than NPB plants (Supplementary Figure S4K, L, O and P). In contrary, *GFP-APIP5nls* transgenic plants exhibited more resistance to RB22 and RB22-*AvrPiz-t* (Supplementary Figure S4M and N). As expected, the defense-associated gene *OsCHITINASE3* was significantly upregulated in *GFP-APIP5nls* plants but downregulated in *GFP-APIP5* and *GFP-APIP5nes* plants compared to NPB (Figure 1F, I and L). Taken together, these results indicate that the NLS in APIP5 also plays an important role in the defense response to *M. oryzae*.

APIP5 accumulation in the nucleus is associated with plant development and blast infection

The importance of the NLS in APIP5 suggested that APIP5 might undergo nucleocytoplasmic trafficking during plant development. To examine this, we analyzed GFP-APIP5 protein abundance in the nucleus and cytoplasm in *GFP-APIP5* plants at the seedling and tillering stages. Immunoblot of the nuclei-enriched fraction and confocal image analyses revealed that GFP-APIP5 mainly accumulated in the nucleus at the tillering stage but not the seedling stage (Figure 2A and Supplementary Figure S5A). By contrast, GFP-APIP5nls mainly localized to the cytoplasm at both the seedling and tillering stages (Figure 2B and Supplementary Figure S5B). We transiently expressed *APIP5* fused with an N-terminal *GFP* tag under the control of the 35S promoter in 1- and 2-month-old *N. benthamiana*. Both confocal image analysis and western blotting consistently showed that GFP-APIP5 was predominantly expressed in the cytoplasm in 1-month-old leaves, whereas a portion of GFP-APIP5 translocated into the nucleus in 2-month-old leaves (Figure 2C and D).

Given that AvrPiz-t targets APIP5 during blast infection (26), we reasoned that activated APIP5 might translocate into the nucleus to act on defense activation. To examine this possibility, we inoculated *GFP-APIP5* plants with *M. oryzae* strain RO1-1 and investigated the nucleocytoplasmic distribution of APIP5 during blast infection. More GFP-APIP5 accumulated in the nuclear pools at 1, 2, and 3 day after inoculation (DAI) compared to the control, but GFP-APIP5 decreased to basal levels at 4 DAI (Figure 2E). Interestingly, APIP5 accumulated rapidly in the cytoplasm at 1 DAI but reduced at 5 DAI (Figure 2E). These results suggest that plant development and blast infection induce the trafficking of APIP5 from the cytoplasm into the nucleus during the early stage of infection.

APIP5 directly targets the cell wall-associated defense gene *OsWAK5*

To identify the target genes regulated by APIP5, we performed an *in vitro* chromatin immunoprecipitation-sequencing (ChIP-seq) experiment using anti-GST antibody against GST-APIP5 (30). In total, we identified 4810 GST-APIP5 binding peaks (corresponding to 880 genes) and 84 GST binding peaks (corresponding to 4 genes), respectively (Supplementary Figure S6A). Genome-wide distribution analysis revealed that the APIP5 binding sites were highly enriched in the promoter region (3 kb upstream of the transcription start site), which accounted for about 64% of all peaks (Supplementary Figure S6B). Gene Ontology analysis further revealed that the specific APIP5 targeting genes were enriched in several biological pathways such Catabolic process, DNA metabolic process and RNA binding (Supplementary Figure S6C). KEGG pathway enrichment showed that APIP5 specific targeted genes were associated with 2-oxocarboxylic acid metabolism, RNA degradation and biosynthesis of amino acids (Supplementary Figure S6D). *De novo* motif analyses revealed that YTTYYTT is the best enriched putative transcription factor binding elements under APIP5 binding peaks (Supplementary Figure S6E). Then we used electrophoretic mobility shift assay (EMSA) to confirm the binding by APIP5 (Supplementary Figure S6E). Among the identified candidate genes, we selected *OsWAK5* for further analysis because the YTTYYTT motif was identified in the promoter of *OsWAK5*, and WAK proteins play critical roles in rice immunity (40,41).

To confirm that APIP5 targets the *OsWAK5* promoter (*OsWAK5Pro*), we designed P1 and P2 probes based on the predicted promoter sequence of *OsWAK5* for an EMSA. MBP-APIP5 specifically bound to P1 and P2, but not MBP (Figure 3A and Supplementary Figure S7A). Interestingly, MBP-APIP5nls showed very little binding to P1 and P2, and the binding activities of MBP-APIP5nes to P1 and P2 were comparable to that of MBP-APIP5 (Supplementary Figure S7B and C). To confirm the *in vitro* data, we performed ChIP-qPCR assays using *APIP5* transgenic plants. The *OsWAK5Pro* region was markedly enriched in *GFP-APIP5nes* and slightly in *GFP-APIP5* plants at the tillering stage but not in *GFP-APIP5nls* plants (Figure 3B). These

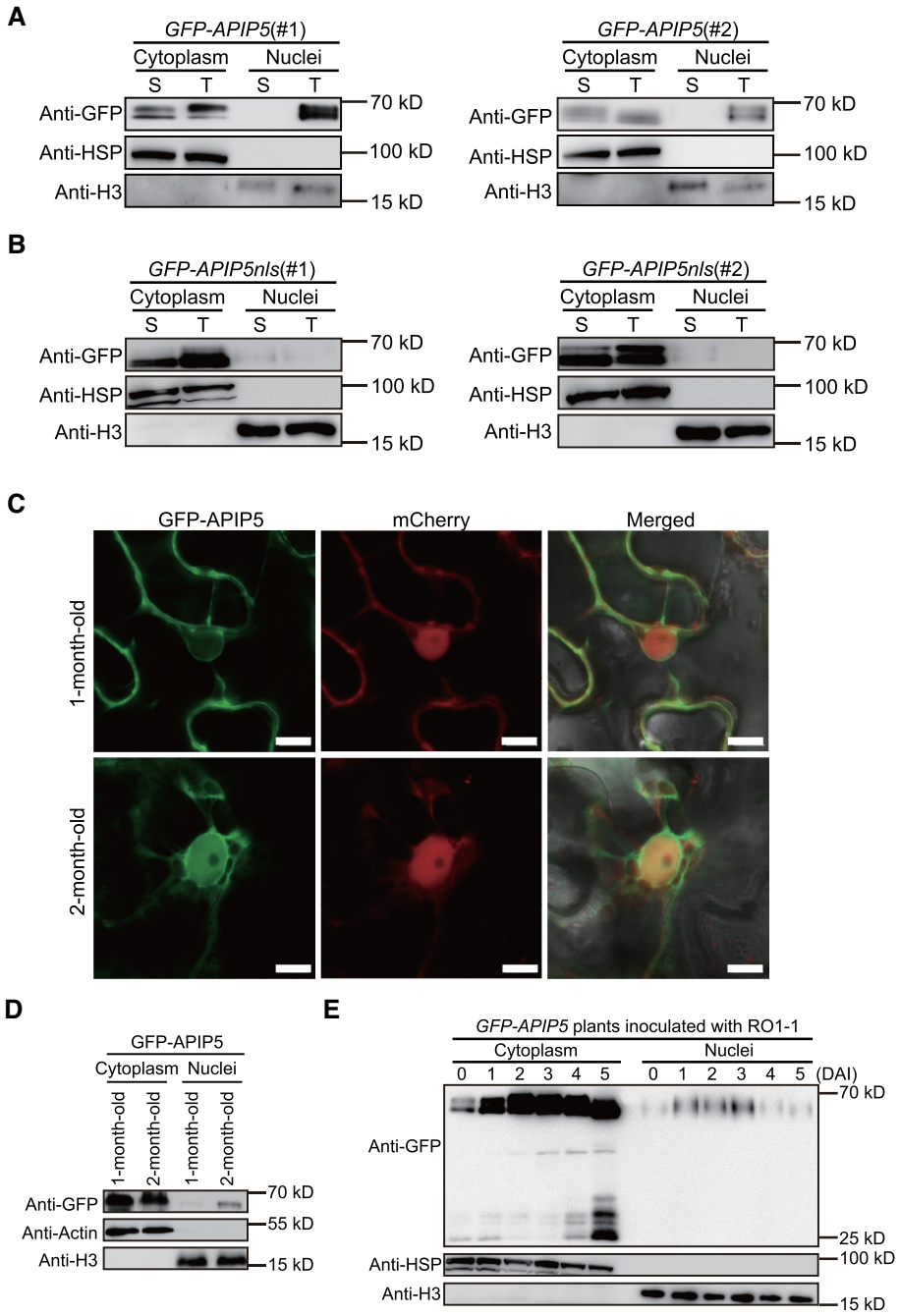

Figure 2. Developmental- and pathogen-dependent nuclear accumulation of GFP-APIP5. (**A**) GFP-APIP5 abundance in cytosolic- and nuclei-enriched fractions from *GFP-APIP5* transgenic plants at the seedling and tillering stages. S represents the seedling stage; T represents the tillering stage. Histone H3 served as a nuclear marker and HSP as a cytosolic marker. The experiment was repeated twice (biological replicates) with similar results, and the representative data from one replicate are shown. (**B**) GFP-APIP5nls abundance in cytosolic- and nuclei-enriched fractions from *GFP-APIP5nls* transgenic plants at the seedling and tillering stages. S represents the seedling stage; T represents the tillering stage. Histone H3 served as a nuclear marker and HSP as a cytosolic marker. The experiment was repeated twice (biological replicates) with similar results, and the representative data from one replicate are shown. (**C**) Confocal images showing the subcellular localization of GFP-APIP5 transiently expressed in the leaves of 1- and 2-month-old *N. benthamiana* plants. mCherry was used a whole-cell localization marker. Scale bars represent 20 μm. (**D**) GFP-APIP5 abundance in cytosolic- and nuclei-enriched fractions from 1- to 2-month-old *N. benthamiana* plants. Histone H3 served as a nuclear marker and Actin as a cytosolic marker. The experiment was repeated twice (biological replicates) with similar results, and the representative data from one replicate are shown. (**E**) GFP-APIP5 abundance in cytosolic- and nuclei-enriched fractions from 3-week-old *GFP-APIP5* transgenic plants after inoculation with RO1-1. DAI represents day after inoculation. The experiment was repeated twice (biological replicates) with similar results, and the representative data from one replicate are shown.

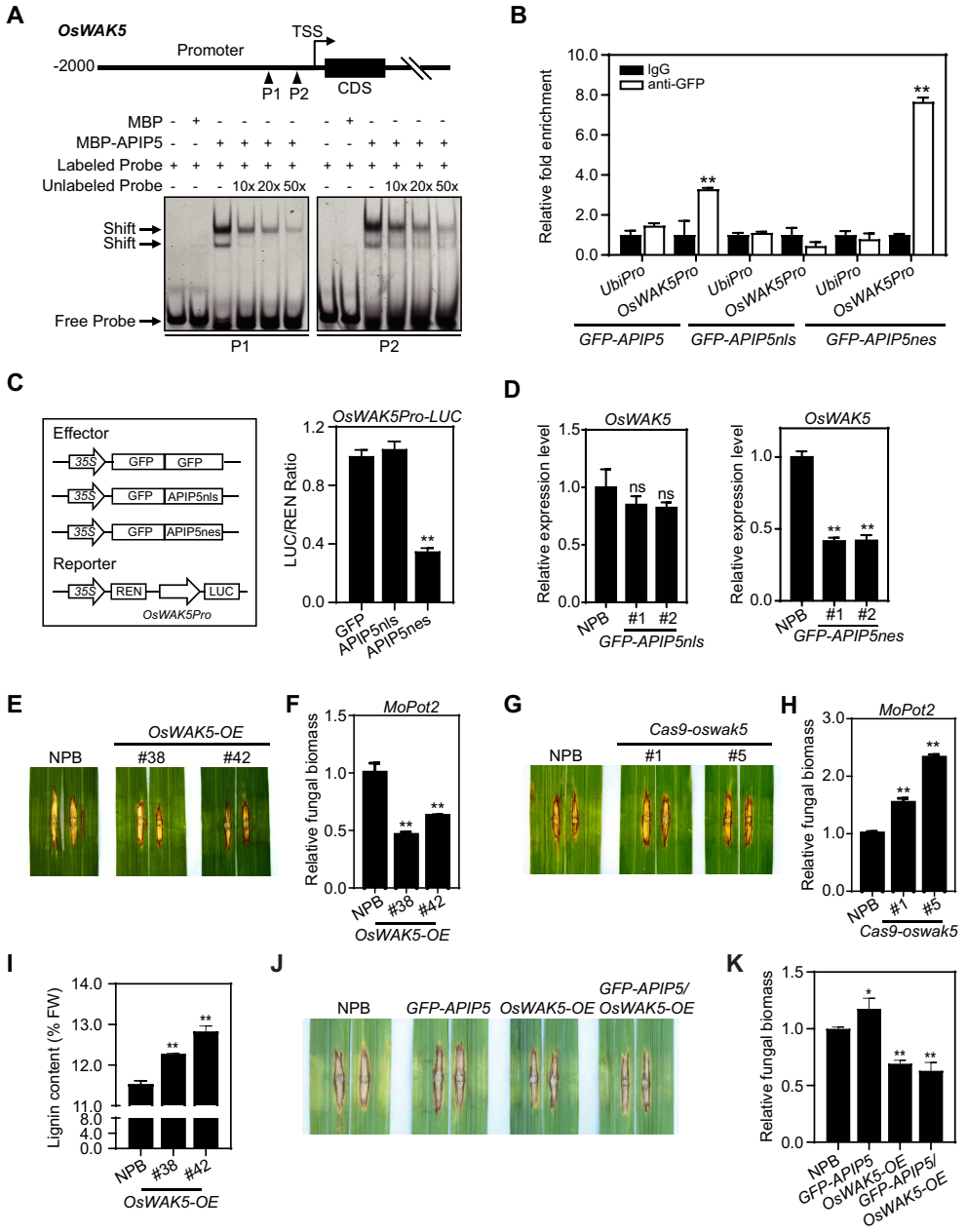

Figure 3. Targeting and suppression of *OsWAK5* by APIP5 and the disease phenotypes of *OsWAK5* overexpression and knock out plants. (**A**) Binding of MBP-APIP5 to the P1 and P2 probes in the *OsWAK5* promoter in an EMSA. MBP alone served as a control. The experiment was repeated three times (biological replicates) with similar results, and the representative data from one replicate are shown. (**B**) ChIP-qPCR of the binding of GFP-APIP5 and GFP-APIP5nes to the *OsWAK5* promoter in transgenic plants at the tillering stage. Similar results were obtained from three independent experiments (biological replicates), and the representative data from one replicate are shown. Values are means ± SE ($n = 3$, technical repeats). (**C**) Luciferase reporter assays of APIP5nes-induced suppression of *OsWAK5Pro* expression in *N. benthamiana*. LUC activity was measured by normalizing to REN signal. Similar results were obtained from three independent experiments (biological replicates) with similar results, and the representative data from one replicate are shown. Values are means ± SE ($n = 3$, technical repeats). (**D**) qRT-PCR analysis of *OsWAK5* expression in *GFP-APIP5nls* and *GFP-APIP5nes* and plants. *UBIQUITIN* (*UBI*) was used as an internal control. Values are means ± SE ($n = 3$, technical repeats). The mean and SE values were obtained from three biological samples (one leaf disc each). (**E** and **F**) Disease symptoms and relative fungal biomass of representative leaves of *OsWAK5*-overexpression and NPB plants after punch inoculation with *M. oryzae* isolate RO1-1. The images were taken at 14 d after inoculation. Similar results were obtained from three independent experiments (biological replicates), and the representative data from one replicate are shown. Values are means ± SE ($n = 3$, technical repeats). The mean and SE values were obtained from five samples. *OsWAK5-OE* plants represent *OsWAK5*-overexpression plants. (**G** and **H**) Disease symptoms and relative fungal biomass of representative leaves of *Cas9-oswak5* and NPB plants after punch inoculation with *M. oryzae* isolate RO1-1. The images were taken at 14 d after inoculation. Similar results were obtained from three independent experiments (biological replicates), and the representative data from one replicate are shown. Values are means ± SE ($n = 3$, technical repeats). The mean and SE values were obtained from five samples. (**I**) Lignin contents of *OsWAK5*-overexpression and NPB plants. Values are means ± SE ($n = 3$, technical repeats). The mean and SE values were obtained from more than five biological samples. (**J** and **K**) Disease symptoms and relative fungal biomass of representative leaves of *GFP-APIP5*, *OsWAK5-OE*, *GFP-APIP5*/*OsWAK5-OE* and NPB plants after punch inoculation with *M. oryzae* isolate RO1-1. Asterisks represent significance levels determined by Student's *t*-test (**$P < 0.01$) compared to the negative controls.

results indicate that the nls mutation in APIP5 may affect its nuclear localization and DNA binding activity to the *OsWAK5* promoter.

Next, we performed a dual-luciferase reporter assay to dissect the role of APIP5 in regulating *OsWAK5* expression. Because of the localization of GFP-APIP5 mainly in cytoplasm and slightly enrichment in *OsWAK5Pro*, we co-expressed the *OsWAK5Pro*::LUC reporter with *GFP*, *GFP-APIP5nls* or *GFP-APIP5nes* in *N. benthamiana* plants (Figure 3C). Compared to GFP, the luciferase-to-Renilla (LUC/REN) ratio decreased in the presence of GFP-APIP5nes, whereas there were no significant differences in the presence of GFP and GFP-APIP5nls (Figure 3C). Consistent with the LUC/REN data, ChIP-qPCR assays showed that GFP-APIP5nes was enriched in the *OsWAK5Pro* region in *N. benthamiana* plants, whereas GFP-APIP5nls were not (Supplementary Figure S7D). We then evaluated the expression of *OsWAK5* in *GFP-APIP5nls* and *GFP-APIP5nes* plants at the tillering stage. *OsWAK5* was significantly downregulated in *GFP-APIP5nes* plants but not in *GFP-APIP5nls* plants compared to NPB (Figure 3D). Collectively, these data suggest that APIP5 targets *OsWAK5* to negatively regulate its expression in the nucleus.

To validate the role of *OsWAK5* in blast resistance, we generated *OsWAK5*-overexpression lines (*OsWAK5-OE*, independent lines #38 and #42) and CRISPR/Cas9 mutants (*Cas9-oswak5*, independent lines #1 and #5) (Supplementary Figure S7E and F) and evaluated their resistance to *M. oryzae*. Compared with NPB, *OsWAK5-OE* plants showed elevated resistance to *M. oryzae* isolate RO1-1, with smaller lesions and reduced fungal biomass (Figure 3E and F), whereas *Cas9-oswak5* mutants displayed reduced resistance to RO1-1, with larger lesions and greater fungal biomass (Figure 3G and H). Moreover, the defense-associated gene *OsCHITINASE3* was significantly upregulated in *OsWAK5-OE* plants but downregulated in *Cas9-oswak5* plants compared to NPB (Supplementary Figure S7G and H).

Cellulose and lignin are the main components of cell walls and involved in the resistance to rice pathogens. For example, the resistance gene *Xa4* encodes a WAK protein that promotes cellulose synthesis to enhance resistance against *Xoo* (40) and OsMYB30 positively regulates the resistance to *M. oryzae* by enhancing the accumulations of lignin (42). These findings prompted us to analyze the cellulose and lignin contents in the *OsWAK5-OE* plants. The cellulose contents were comparable in *OsWAK5-OE* and NPB plants (Supplementary Figure S7I), while the lignin contents were much higher in the *OsWAK5-OE* plants than in NPB (Figure 3I). To further confirm the genetic relationship between *OsWAK5* and *APIP5*, we generated the *GFP-APIP5*/*OsWAK5-OE* hybrid plants by genetic crossing of the *GFP-APIP5* plants with *OsWAK5-OE* plants (Supplementary Figure S7J). Similar with the *OsWAK5-OE* plants, *GFP-APIP5*/*OsWAK5-OE* plants displayed more resistance to isolate RO1-1, with smaller lesions and reduced fungal biomass (Figure 3J and K). Together, these results demonstrate that APIP5 suppresses the expression of *OsWAK5*, which positively regulates resistance to *M. oryzae* by inducing defense gene expression and promoting lignin biosynthesis.

APIP5 directly targets the cytochrome P450 defense gene *CYP72A1*

Cytochrome P450 enzymes (CYPs) participate in the biosynthesis and catabolism of phytohormones, antioxidants and defense compounds (43,44). CYP72s comprise one of the largest subgroups of CYPs (45). We identified *CYP72A1* in the *in vitro* ChIP-seq assay described above and *CYP72A1* contains a YTTYYTT motif in its promoter. Therefore, in addition to *OsWAK5*, we focused on *CYP72A1* as a potential target gene. To assess whether APIP5 binds to the *CYP72A1* promoter (*CYP72A1Pro*), we performed EMSA. Both MBP-APIP5 and MBP-APIP5nes specifically bound to P1 and P2 in the *CYP72A1* promoter, whereas MBP-APIP5nls showed little binding to P1 and P2 (Figure 4A and Supplementary Figure S8A–C). ChIP-qPCR assays indicated that the *CYP72A1Pro* region was significantly enriched in *GFP-APIP5nes* plants and slightly in *GFP-APIP5* plants at the tillering stage but not in *GFP-APIP5nls* plants (Figure 4B). These results indicate that the nls mutation in APIP5 may affect its nuclear localization and DNA binding activity to the *CYP72A1* promoter.

Because of the localization of GFP-APIP5 mainly in cytoplasm and slightly enrichment in *CYP72A1Pro*, we co-expressed the *CYP72A1Pro*::LUC reporter with *GFP*, *GFP-APIP5nls* or *GFP-APIP5nes* in *N. benthamiana* plants, the results showed that GFP-APIP5nes repressed the LUC activity of *CYP72A1Pro*, whereas GFP and GFP-APIP5nls did not (Figure 4C). Indeed, ChIP-qPCR revealed that GFP-APIP5nes was enriched at *CYP72A1Pro* in *N. benthamiana* plants (Supplementary Figure S8D). We analyzed the expression levels of *CYP72A1* in *GFP-APIP5nls* and *GFP-APIP5nes* plants at the tillering stage. *CYP72A1* was significantly downregulated in *GFP-APIP5nes* plants, but there were no significant differences in *CYP72A1* expression between *GFP-APIP5nls* and NPB plants (Figure 4D). These results indicate that APIP5 binds to the *CYP72A1* promoter to negatively regulate its expression following *M. oryzae* infection.

To determine the role of *CYP72A1* in blast resistance, we generated *CYP72A1*-overexpression lines (*CYP72A1-OE*, independent lines #8 and #9) and CRISPR/Cas9 mutants (*Cas9-cyp72a1*, independent lines #1 and #2) (Supplementary Figure S8E and F) and evaluated their resistance to *M. oryzae*. Compared to NPB, *CYP72A1-OE* plants were more resistant to RO1-1, with smaller disease lesions and less fungal biomass (Figure 4E and F), whereas *Cas9-cyp72a1* plants were more susceptible to this pathogen, with larger disease lesions and greater fungal biomass (Figure 4G and H). The defense-associated gene *OsCHITINASE3* was significantly upregulated in *CYP72A1-OE* plants but downregulated in *Cas9-cyp72a1* plants compared to NPB (Supplementary Figure S8G and H).

CYPs are heme-containing enzymes involved in various oxidation-reduction reactions (46); therefore, we analyzed whether CYP72A1 affects cytochrome *c* metabolism in rice. COX is the last electron acceptor of the mitochondrial respiratory chain, which is associated with ROS generation (47,48). We found that COX IV activity was much lower in *CYP72A1-OE* plants than in NPB (Figure 4I). Moreover, the ROS burst in *CYP72A1-OE* plants were more ro-

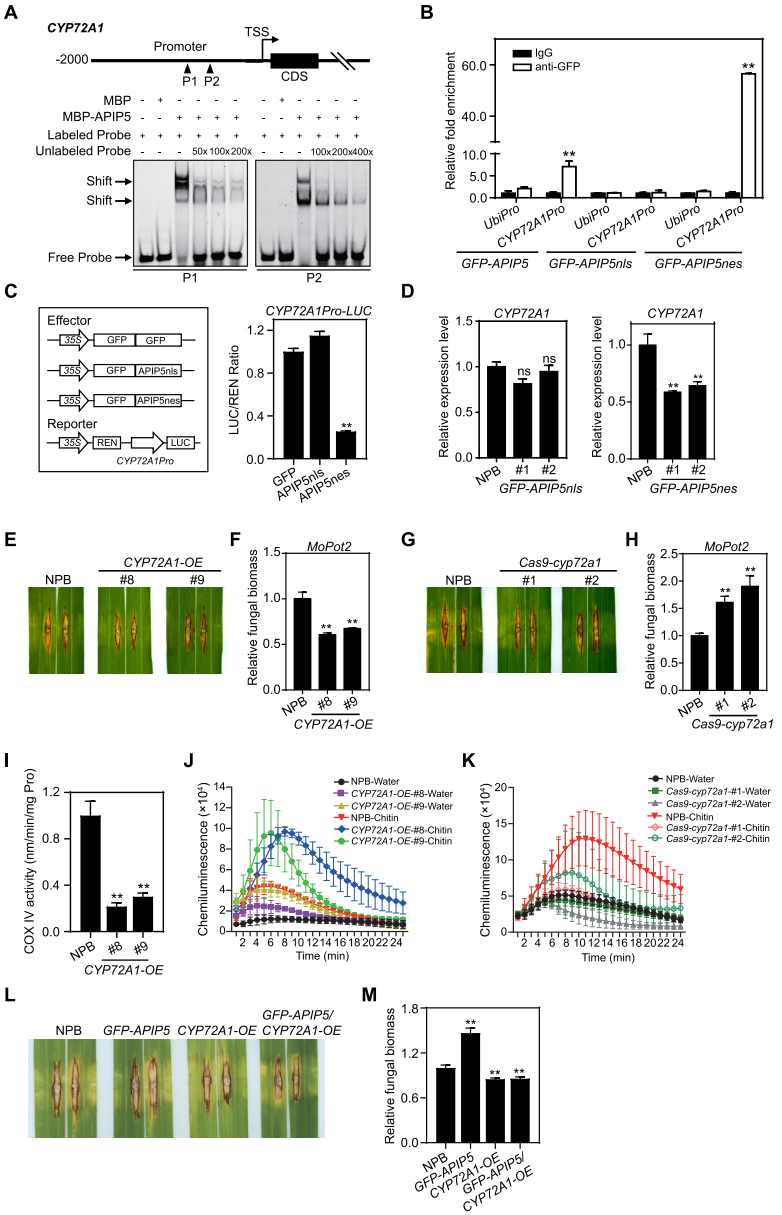

Figure 4. Targeting and suppression of *CYP72A1* by APIP5 and the disease phenotypes of *CYP72A1* overexpression and knockout plants. (**A**) MBP-APIP5 binding to P1 and P2 probes of the *CYP72A1* promoter in an EMSA. MBP alone served as a control. The experiment was repeated three times (biological replicates) with similar results, and the representative data from one replicate are shown. (**B**) ChIP-qPCR analysis of GFP-APIP5 and GFP-APIP5nes binding to the *CYP72A1* promoter in transgenic plants at the tillering stage. Similar results were obtained from three independent experiments (biological replicates), and the representative data from one replicate are shown. Values are means ± SE ($n = 3$, technical repeats). (**C**) Luciferase reporter assays of APIP5nes-induced suppression of *CYP72A1* expression in *N. benthamiana*. LUC activity was measured by normalizing to the REN signal. Similar results were obtained from three independent experiments (biological replicates) with similar results, and the representative data from one replicate are shown. Values are means ± SE ($n = 3$, technical repeats). (**D**) qRT-PCR analysis of *CYP72A1* expression in *GFP-APIP5nls* and *GFP-APIP5nes* plants. *UBIQUITIN* (*UBI*) was used as an internal control. Values are means ± SE ($n = 3$, technical repeats). The mean and SE values were obtained from three biological samples (one leaf disc each). (**E** and **F**) Disease symptoms and relative fungal biomass of representative leaves of *CYP72A1*-overexpression and NPB plants after punch inoculation with *M. oryzae* isolate RO1-1. The images were taken at 14 d after inoculation. Similar results were obtained from three independent experiments (biological replicates), and the representative data from one replicate are shown. Values are means ± SE ($n = 3$, technical repeats). The mean and SE values were obtained from five samples. *CYP72A1-OE* represents *CYP72A1*-overexpression plants. (**G** and **H**) Disease symptoms and relative fungal biomass of representative leaves of *Cas9-cyp72a1* and NPB plants after punch inoculation with *M. oryzae* isolate RO1-1. The images were taken at 14 d after inoculation. Similar results were obtained from three independent experiments (biological replicates), and the representative data from one replicate are shown. Values are means ± SE ($n = 3$, technical repeats). The mean and SE values were obtained from five samples. (**I**) Cytochrome *c* oxidase activity in *CYP72A1*-overexpression and NPB plants. Values are means ± SE ($n = 3$, technical repeats). The mean and SE values were obtained from more than three biological samples (one leaf each). ROS burst induced by chitin in *CYP72A1-OE* (**J**) and *Cas9-cyp72a1* (**K**) leaves. The leaf discs of *CYP72A1-OE*, *Cas9-cyp72a1* and NPB plants were treated with 8 nM chitin. Values are means ± SE ($n = 3$, biological repeats). (**L** and **M**) Disease symptoms and relative fungal biomass of representative leaves of *GFP-APIP5*, *CYP72A1-OE*, *GFP-APIP5*/*CYP72A1-OE* and NPB plants after punch inoculation with *M. oryzae* isolate RO1-1. Asterisks represent significance levels determined by Student's *t*-test (*$P < 0.05$, **$P < 0.01$) compared to the negative controls.

bust than that in NPB after treatment with chitin, while ROS burst in *Cas9-cyp72a1* mutants were much weaker than that in NPB (Figure 4J and K). CYPs were reported in the biosynthesis and catabolism of antioxidants and defense compounds (43,49). We therefore analyzed the non-targeted metabolite profiling in *CYP72A1-OE* plants. The result showed that some defense compounds were significantly increased in *CYP72A1-OE* plants than in NPB plants, such as Oryzalexin S, Momilactone B, Oryzalexin C and so on (Supplementary Figure S8I). Meanwhile, other compounds, like Oryzalexin F(17)-H_2O, Diosgenin and Manglieside E, were significantly decreased in *CYP72A1-OE* plants than in NPB plants (Supplementary Figure S8I).

To confirm the genetic relationship between CYP72A1 and APIP5, we crossed *GFP-APIP5* plants with *CYP72A1-OE* plants to generate *GFP-APIP5*/*CYP72A1-OE* plants (Supplementary Figure S8J). Similar with *CYP72A1-OE* plants, *GFP-APIP5*/*CYP72A1-OE* plants displayed more resistance to isolate RO1-1, with smaller lesions and reduced fungal biomass (Figure 4L and M). Collectively, these results suggest that APIP5 directly suppresses the expression of *CYP72A1* and thus regulates ROS and defense compounds accumulations in rice during *M. oryzae* infection.

APIP5 functions as an RNA-binding protein to regulate the cell death and defense response genes *OsLSD1* and *OsRac1*

When the *GFP-APIP5* plasmids were transiently expressed in rice protoplasts, we observed a few bright spots in the cytoplasm (Figure 5A). These bright spots co-localized with the processing body (P-body) markers NbDCP1 and NbDCP2, which recognize some RNAs and target them for turnover (50,51) (Figure 5A). Strikingly, the P-body localization in GFP-APIP5 was significantly increased in *GFP-APIP5* sheath epidermal cells at 48 h after infection with RO1-1 (Supplementary Figure S9A). These findings suggest that APIP5 may selectively associate with some RNA transcripts in the cytoplasm.

To assess whether APIP5 binds to RNA, we performed *in vitro* RNA binding assays using recombinant MBP-APIP5 fusion proteins and homopolymers of A, U and C. As a control, we used OsTZF1, a CCCH-type zinc finger protein that directly binds to U-rich regions in the 3′untranslated regions (UTRs) of mRNAs (52). An RNA EMSA (REMSA) showed that APIP5 strongly bound to poly(U) and weakly bound to poly(C) (Figure 5B; Supplementary Figure S9B and C), like the control OsTZF1. The binding activity of MBP-APIP5 to poly(U) probe was out-competed by unlabeled poly(U) probe (Figure 5C and Supplementary Figure S9D), and this activity was partially competed by unlabeled DNA motif (YTTYYTT) probe (Supplementary Figure S9E), indicating that there may be some cross-talk between RNA binding and DNA binding of APIP5. Interestingly, MBP-APIP5nls and MBP-APIP5nes showed almost no binding activity with poly(U) (Figure 5D and E, Supplementary Figure S9F and G). These results suggest that APIP5 functions as an unconventional RNA-binding protein selectively with some RNA transcripts in cytoplasmic foci, which may be influenced by some amino acids in the NLS and NES motifs.

To identify mRNAs that are regulated by APIP5, we searched for poly(U)-enriched mRNA transcripts of genes known to be involved in defense responses. The 3′UTRs of *OsLSD1* and *OsRac1* were enriched with poly(U) (Supplementary Figure S10). OsLSD1 negatively regulates PCD and is involved in the defense response to *M. oryzae* (53). OsRac1, a small GTPase, is associated with ROS production, PCD and plant immunity (54,55). To determine whether APIP5 binds to the 3′UTRs of *OsLSD1* and *OsRac1*, we performed REMSAs and confirmed that biotinylated *OsLSD1* and *OsRac1* 3′UTRs were able to pull down MBP-APIP5 but not MBP (Figure 6A and B). In *in vitro* RIP assays, MBP-APIP5 was substantially enriched in *OsLSD1* and *OsRac1* mRNA, whereas MBP was not (Figure 6C). We then performed an *in vivo* RIP assay using *GFP-APIP5* transgenic plants. We designed primers for qPCR in the A and C regions of *OsLSD1* and *OsRac1*, which are poor in poly(U), as negative controls (Figure 6D). GFP-APIP5 was specifically enriched with *OsLSD1* and *OsRac1* mRNA, especially in the 3′UTRs (Figure 6D). These results demonstrate that APIP5 directly binds to *OsLSD1* and *OsRac1* mRNA *in vitro* and *in vivo*.

Finally, we analyzed the mRNA turnover rates of *OsLSD1* and *OsRac1* in *Cas9-apip5* and *GFP-APIP5* plants. We designed primers for qPCR to detect the 5′- and 3′-ends of *OsLSD1* and *OsRac1* mRNA, respectively. The ratio of 5′- to 3′-ends of *OsLSD1* was significantly lower in *Cas9-apip5* and much higher in *GFP-APIP5* plants compared to NPB, as determined by qPCR (Figure 6E). Similarly, the ratio of 5′- to 3′-ends of *OsRac1* was lower in *Cas9-apip5* and slightly higher in *GFP-APIP5* plants than in NPB (Figure 6F). In addition, the ratio of 5′- to 3′-ends of *OsLSD1* rapidly increased in NPB after inoculation by *M. oryzae* at 1 d, but not in the *Cas9-apip5* mutant (Supplementary Figure S11A), and the ratio of 5′- to 3′-ends of *OsRac1* reached its highest level at 5 d after *M. oryzae* inoculation in NPB plants, while no changes in the *Cas9-apip5* mutant (Supplementary Figure S11B). Together, these results demonstrate that APIP5 functions as an RNA-binding protein to regulate the expression of the defense-related genes *OsLSD1* and *OsRac1* at the post-transcriptional level.

DISCUSSION

Emerging evidence in animal systems shows that, in addition to their roles in regulating gene expression, TFs bind to different types of RNA and regulate RNA turnover (19,20). However, whether plant TFs have similar functions is still unknown. In the current study, we discovered that APIP5, a negative regulator of plant defense responses, translocates from the cytoplasm to the nucleus to directly target *OsWAK5* and *CYP72A1* and suppress their expression, thereby reducing lignin contents and ROS accumulation during *M. oryzae* infection. Strikingly, in the cytoplasm, APIP5 functions as an unconventional RNA-binding protein that directly binds to *OsLSD1* and *OsRac1* mRNAs and regulates their turnover in response to *M. oryzae*. Our study thus uncovered the first plant bZIP type TF with dual functions in transcriptional regulation and RNA turnover during plant PCD and immunity responses. These findings open an avenue to exploring the molecular mechanisms un-

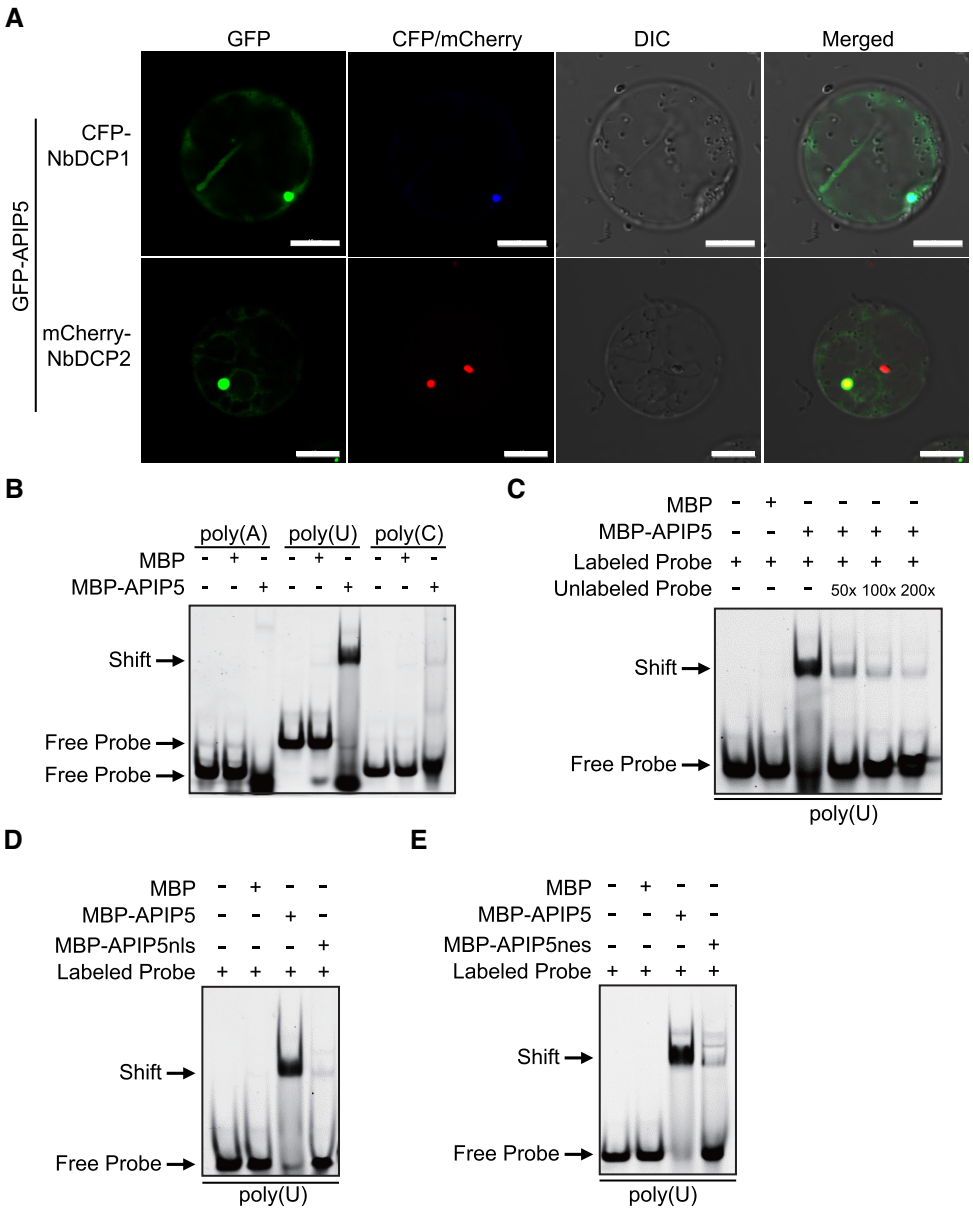

Figure 5. APIP5 functions as a novel RNA-binding protein. (**A**) Co-localization of GFP-APIP5 with CFP-NbDCP1 and mCherry-NbDCP2 in NPB protoplasts. Scale bars represent 10 μm. (**B**) Binding affinity of MBP-APIP5 toward poly(A), poly(U) and poly(C). The experiment was repeated three times (biological replicates) with similar results, and the representative data from one replicate are shown. (**C**) Unlabeled probe competed with the binding activity of MBP-APIP5 with poly(U). Binding activity of MBP-APIP5nls (**D**) and MBP-APIP5nes (**E**) with poly(U).

derlying how plant TFs partition between the nucleus and cytoplasm and how the plant cell coordinates these two activities during defense activation.

WAKs comprise a unique group of receptor like kinases (RLKs) that likely associate with pectin in the cell wall, transduce signals from the cell wall and apoplast to the cytoplasm, and contribute to cell expansion during development and plant responses to pathogens (56,57). The rice genome contains 125 genes encoding WAK-like proteins, including 67 encoding WAK-RLKs. The disease resistance gene *Xa4* encodes a WAK that promotes cellulose synthesis and strengthens the plant cell wall, thus enhancing plant resistance against *Xoo* infection and lodging (40). In the current study, we demonstrated that *OsWAK5* is a target of APIP5 and that overexpressing *OsWAK5* enhances blast resistance and promotes lignin synthesis. Upon pathogen infection, some cytoplasmic APIP5 protein translocates into the nucleus where it might bind to the promoter of *OsWAK5* to suppress its expression. GhWAK7A functions in the resistance of cotton (*Gossypium hirsutum*) to *Fusarium oxysporum* f. sp. *vasinfectum* and *Verticillium dahliae* by interacting with both GhCERK1 and GhLYK5 and phosphorylating GhLYK5 to induce chitin-induced responses (58). In tomato (*Solanum lycopersicum*), SlWak1 acts as an important positive regulator during the late stages of flagellin-mediated PTI responses in the apoplast and associates with

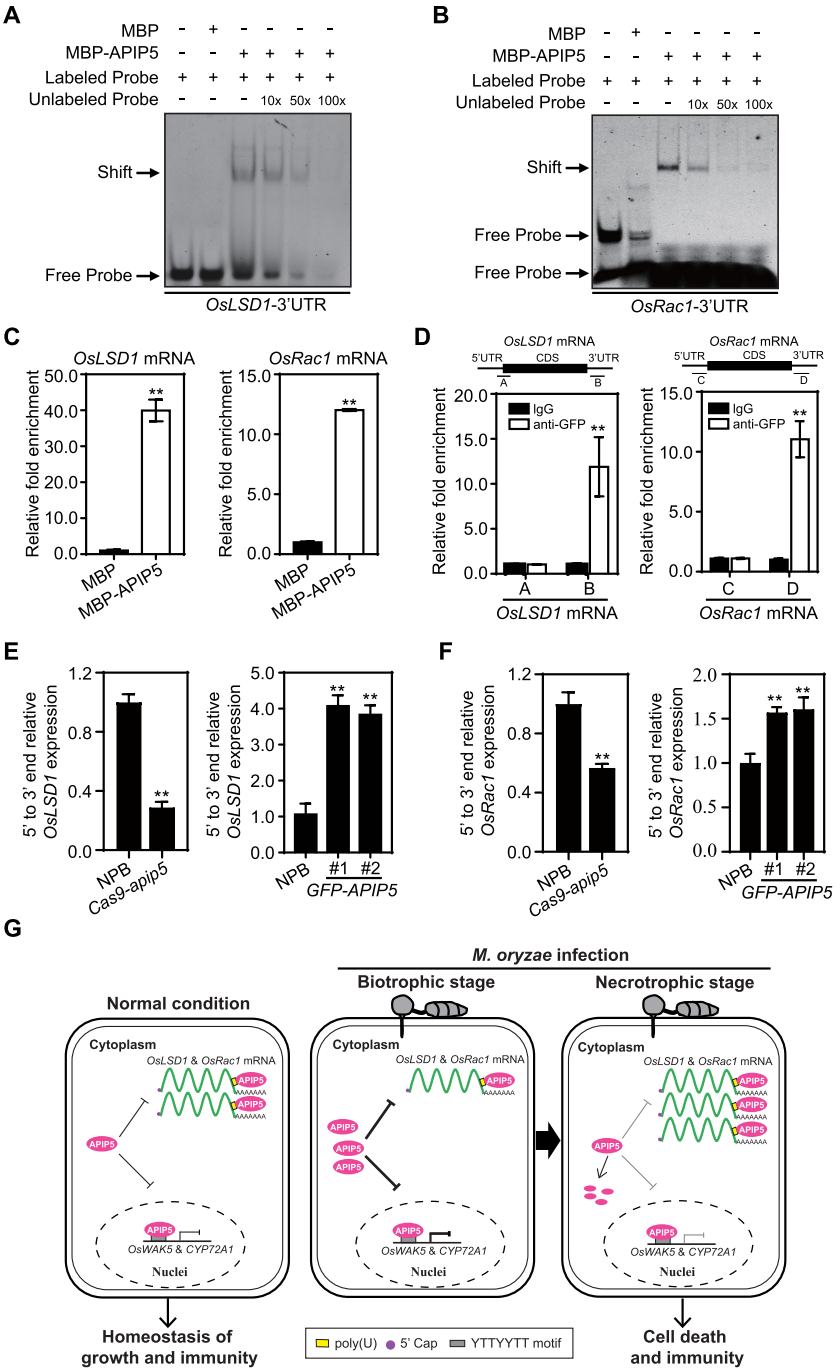

Figure 6. APIP5 binds to *OsLSD1* and *OsRac1* mRNAs and regulates their turnover. (**A**) Binding activity of MBP-APIP5 with *OsLSD1*-3′UTR in a REMSA. The experiment was repeated three times (biological replicates) with similar results, and the representative data from one replicate are shown. (**B**) Binding activity of MBP-APIP5 with *OsRac1*-3′UTR in a REMSA. The experiment was repeated three times (biological replicates) with similar results, and the representative data from one replicate are shown. (**C**) qRT-PCR analysis of *OsLSD1* and *OsRac1* mRNA enrichment in *in vitro* RIP experiments. Relative enrichment was calculated as the fold change of RNA abundance following pull-down by MBP-APIP5 vs. MBP. The experiment was repeated twice (biological replicates) with similar results, and the representative data from one replicate are shown. Values are means ± SE ($n = 3$, technical repeats). (**D**) *In vivo* RIP assays of GFP-APIP5 binding to *OsLSD1* and *OsRac1* mRNAs in *GFP-APIP5* transgenic plants. The experiment was repeated twice (biological replicates) with similar results, and the representative data from one replicate are shown. Values are means ± SE ($n = 3$, technical repeats). In the diagram of *OsLSD1* and *OsRac1* mRNA structures, the line represents the untranslated region (UTR), and the black box represents the coding sequence (CDS) region. A, B, C and D are the sequence regions used for the RIP assays. (**E**) *OsLSD1* mRNA turnover rates in *Cas9-apip5*, *GFP-APIP5* and NPB plants. Values are means ± SE ($n = 3$, technical repeats). The mean and SE values were obtained from three biological samples (one leaf disc each). (**F**) *OsRac1* mRNA turnover rates in *Cas9-apip5*, *GFP-APIP5* and NPB plants. Values are means ± SE ($n = 3$, technical repeats). The mean and SE values were obtained from three biological samples (one leaf disc each). (**G**) A working model illustrating the molecular mechanism of *APIP5*-mediated cell death and immunity to *M. oryzae* in rice. See details in the Discussion section. Asterisks represent significance levels determined by Student's *t*-test (**$P < 0.01$) compared to the negative controls or NPB.

FLAGELLIN SENSITIVE2 (FLS2) and FLS3 to trigger immune signaling (59). Thus, OsWAK5 may act as a co-receptor with OsCERK1 and OsLYP4/6 to perceive chitin (60,61), which leads to the delivery of signals to downstream defense pathways and enhances lignin biosynthesis.

CYPs function in secondary metabolism, development and plant responses to pathogens (45,49). The CYP72A subgroup is one of the largest groups of P450s, which are recruited for the biosynthesis of monoterpene indole alkaloids and triterpenoids (46). Suppressing the expression of *TaCYP72A* in wheat (*Triticum aestivum*) via gene silencing significantly reduced plant tolerance to mycotoxin deoxynivalenol (62). In barberry (*Berberis vulgaris*), BvCYP72A552 catalyzes the formation of hederagenin-based saponins to mediate plant defense responses against herbivores (63). In *Catharanthus roseus*, CYP72A1 catalyzes the early step of the indole alkaloid biosynthesis pathway (64). In rice, *CYP72A18*, *CYP72A19*, *CYP72A22* and *CYP72A23* are differentially regulated during the incompatible and compatible interactions between rice and *M. oryzae* (65). However, the biological functions of CYP72As are poorly understood, especially their roles in coordination with secondary metabolism and plant immunity and their regulatory mechanisms. In the current study, we demonstrated that CYP72A1 is a positive regulator of blast resistance and that APIP5 directly targets *CYP72A1* to inhibit its expression, thereby comprising plant defense. Intriguingly, *CYP72A1*-overexpression plants had higher COX IV activity, stronger ROS burst and accumulated more defense-related secondary metabolism than NPB, suggesting that CYP72A1 may promote ROS burst through defense compound accumulation in rice immunity.

Proteins containing CCCH motif-, RRM- or TRP-containing domains are associated with RNA processing (66). The roles of a few such proteins in plant immunity have been elucidated, such as AtTZF9, Bsr-k1, and PIBP1 (25,36,67). In the current study, we demonstrated that APIP5 co-localizes with NbDCP1 and NbDCP2 and has RNA-binding activity, preferentially for poly(U). Notably, *OsLSD1* and *OsRac1* mRNAs are enriched with poly(U) sequences, especially in their 3′UTRs. In addition, APIP5 directly binds to *OsLSD1* and *OsRac1* mRNAs and regulates their turnover rates during *M. oryzae* infection. In *Arabidopsis*, LSD1 negatively regulates PCD and directly interacts with catalases (CAT1, CAT2 and CAT3) to regulate light-dependent runaway cell death and pathogen-induced cell death (68). OsLSD1 also plays a negative role in PCD and regulates resistance to *M. oryzae* in rice, but the underlying molecular mechanisms are still unknown (53). OsRac1 is involved in PTI and Pit-mediated resistance against *M. oryzae* (69,70). The constitutively active form of OsRac1 increases ROS production and cell death (71) and directly interacts with the N-terminal region of the NADPH oxidase *Oryza sativa* respiratory burst oxidase homolog B (OsRbohB) (55). The mRNA turnover rates of *OsLSD1* and *OsRac1* were much lower in *Cas9-apip5* mutants and significantly higher in *GFP-APIP5* overexpression plants compared to NPB. Therefore, it is likely that APIP5 functions in the cytoplasm to modulate the RNA processing of *OsLSD1* and *OsRac1*, which is essential for the production and metabolism of ROS. Further studies are needed to decipher how APIP5 interacts with and regulates the mRNAs of these two defense genes during immunity responses in rice.

In summary, we characterized the dual roles of APIP5 in regulating PCD and defense responses in rice by functioning as a TF in the nucleus and as a novel RNA-binding protein in the cytoplasm. We propose a working model for the dual roles of APIP5 in PCD and plant immunity (Figure 6G). APIP5 displays development- and pathogen-dependent nucleocytoplasmic shuttling, which may be also regulated by other factors such as light, temperature, humidity and phytohormone. Under normal conditions, APIP5 is predominantly localized to the cytoplasm to control the turnover of *OsLSD1* and *OsRac1* transcripts. A small fraction of APIP5 enters into the nucleus to bind to the promoters of *OsWAK5* and *CYP72A1* and suppress their expression. These two functions are essential to avoid auto-immunity and promote plant growth in the absence of *M. oryzae*. Upon infection with *M. oryzae*, *APIP5* is induced and some of the APIP5 protein in the cytoplasm is translocated into the nucleus during the early stages of infection (Figure 2E). The increased amount of APIP5 in both subcellular compartments leads to the suppression of defense gene transcription and the rapid turnover of defense-related mRNAs, which is beneficial for biotrophic invasion by *M. oryzae* at this stage. However, when the fungal hyphae grow rapidly inside the rice cells, AvrPiz-t and other effectors are secreted into the cells to suppress the transcriptional activity and accumulation of APIP5 (26). During the late stage of infection (approximately 3 days after inoculation), APIP5 levels gradually decrease in the nucleus, and this protein may be also degraded in the cytoplasm during the infection stage (Figure 2E), which leads to increased gene activation, the accumulation of defense-related transcripts and ultimately the inhibition of fungal infection. Nevertheless, the intrinsic regulatory mechanisms underlying the nucleocytoplasmic partitioning of APIP5 and the APIP5-mediated suppression of *OsWAK5* and *CYP72A1* expression and *OsLSD1* and *OsRac1* mRNA turnover warrant further investigation.

DATA AVAILABILITY

The accession number for the data reported in this study is GEO: GSE198135.

SUPPLEMENTARY DATA

Supplementary Data are available at NAR Online.

ACKNOWLEDGEMENTS

We thank Dr Fangfang Li from Institute of Plant Protection, Chinese Academy of Agricultural Sciences for providing *CFP-NbDCP1* and m*Cherry-NbDCP2* plasmids.

FUNDING

National Natural Science Foundation of China [32161143009 to Y.N.; 31801692 to F.Z.]. Funding for open access charge: National Natural Science Foundation of China [32161143009].

Conflict of interest statement. None declared.

REFERENCES

1. Love,A.J., Milner,J.J. and Sadanandom,A. (2008) Timing is everything: regulatory overlap in plant cell death. *Trends Plant Sci.*, **13**, 589–595.
2. Mukhtar,M.S., McCormack,M.E., Argueso,C.T. and Pajerowska-Mukhtar,K.M. (2016) Pathogen tactics to manipulate plant cell death. *Curr. Biol.*, **26**, R608–R619.
3. Gao,M., Wang,X., Wang,D., Xu,F., Ding,X., Zhang,Z., Bi,D., Cheng,Y.T., Chen,S., Li,X. *et al.* (2009) Regulation of cell death and innate immunity by two receptor-like kinases in Arabidopsis. *Cell Host Microbe*, **6**, 34–44.
4. de Oliveira,M.V., Xu,G., Li,B., de Souza Vespoli,L., Meng,X., Chen,X., Yu,X., de Souza,S.A., Intorne,A.C., de,A.M.A.M. *et al.* (2016) Specific control of Arabidopsis BAK1/SERK4-regulated cell death by protein glycosylation. *Nat. Plants*, **2**, 15218.
5. Zhou,J.M. and Zhang,Y.L. (2020) Plant immunity: danger perception and signaling. *Cell*, **181**, 978–989.
6. Withers,J. and Dong,X.N. (2017) Post-translational regulation of plant immunity. *Curr. Opin. Plant Biol.*, **38**, 124–132.
7. Burke,R., Schwarze,J., Sherwood,O.L., Jnaid,Y., McCabe,P.F. and Kacprzyk,J. (2020) Stressed to death: the role of transcription factors in plant programmed cell death induced by abiotic and biotic stimuli. *Front. Plant Sci.*, **11**, 1235.
8. Meier,I. and Somers,D.E. (2011) Regulation of nucleocytoplasmic trafficking in plants. *Curr. Opin. Plant Biol.*, **14**, 538–546.
9. Wang,W.M., Liu,P.Q., Xu,Y.J. and Xiao,S.Y. (2016) Protein trafficking during plant innate immunity. *J. Integr. Plant Biol.*, **58**, 284–298.
10. McLellan,H., Boevink,P.C., Armstrong,M.R., Pritchard,L., Gomez,S., Morales,J., Whisson,S.C., Beynon,J.L. and Birch,P.R. (2013) An RxLR effector from Phytophthora infestans prevents re-localisation of two plant NAC transcription factors from the endoplasmic reticulum to the nucleus. *PLoS Pathog.*, **9**, e1003670.
11. Yan,J.L., Chen,Q.Q., Cui,X., Zhao,P.Y., Gao,S.D., Yang,B., Liu,J.X., Tong,T.T., Deyholos,M.K. and Jiang,Y.Q. (2021) Ectopic overexpression of a membrane-tethered transcription factor gene NAC60 from oilseed rape positively modulates programmed cell death and age-triggered leaf senescence. *Plant J.*, **105**, 600–618.
12. Kaminaka,H., Nake,C., Epple,P., Dittgen,J., Schutze,K., Chaban,C., Holt,B.F. 3rd, Merkle,T., Schafer,E., Harter,K. *et al.* (2006) bZIP10-LSD1 antagonism modulates basal defense and cell death in Arabidopsis following infection. *EMBO J.*, **25**, 4400–4411.
13. Correa,L.G., Riano-Pachon,D.M., Schrago,C.G., Santos,R.V., Mueller-Roeber,B. and Vincentz,M. (2008) The role of bZIP transcription factors in green plant evolution: adaptive features emerging from four founder genes. *PLoS One*, **3**, e2944.
14. Pieterse,C.M. and Van Loon,L.C. (2004) NPR1: the spider in the web of induced resistance signaling pathways. *Curr. Opin. Plant Biol.*, **7**, 456–464.
15. Chai,T.T., Zhou,J., Liu,J. and Xing,D. (2015) LSD1 and HY5 antagonistically regulate red light induced-programmed cell death in Arabidopsis. *Front. Plant Sci.*, **6**, 292.
16. Chen,S.Y., Ma,T., Song,S.R., Li,X.L., Fu,P.N., Wu,W., Liu,J.Q., Gao,Y., Ye,W.X., Dry,I.B. *et al.* (2021) Arabidopsis downy mildew effector HaRxLL470 suppresses plant immunity by attenuating the DNA-binding activity of bZIP transcription factor HY5. *New Phytol.*, **230**, 1562–1577.
17. Chern,M., Xu,Q., Bart,R.S., Bai,W., Ruan,D., Sze-To,W.H., Canlas,P.E., Jain,R., Chen,X.W. and Ronald,P.C. (2016) A genetic screen identifies a requirement for cysteine-rich-receptor-like kinases in rice NH1 (OsNPR1)-Mediated immunity. *PLoS Genet.*, **12**, e1006049.
18. Moon,S.J., Park,H.J., Kim,T.H., Kang,J.W., Lee,J.Y., Cho,J.H., Lee,J.H., Park,D.S., Byun,M.O., Kim,B.G. *et al.* (2018) OsTGA2 confers disease resistance to rice against leaf blight by regulating expression levels of disease related genes via interaction with NH1. *PLoS ONE*, **13**, e0206910.
19. Hudson,W.H. and Ortlund,E.A. (2014) The structure, function and evolution of proteins that bind DNA and RNA. *Nat. Rev. Mol. Cell Biol.*, **15**, 749–760.
20. Holmes,Z.E., Hamilton,D.J., Hwang,T., Parsonnet,N.V., Rinn,J.L., Wuttke,D.S. and Batey,R.T. (2020) The Sox2 transcription factor binds RNA. *Nat. Commun.*, **11**, 1805.
21. Kim,W.C., Kim,J.Y., Ko,J.H., Kang,H., Kim,J. and Han,K.H. (2014) AtC3H14, a plant-specific tandem CCCH zinc-finger protein, binds to its target mRNAs in a sequence-specific manner and affects cell elongation in Arabidopsis thaliana. *Plant J.*, **80**, 772–784.
22. Pomeranz,M.C., Hah,C., Lin,P.C., Kang,S.G., Finer,J.J., Blackshear,P.J. and Jang,J.C. (2010) The Arabidopsis tandem zinc finger protein AtTZF1 traffics between the nucleus and cytoplasmic foci and binds both DNA and RNA. *Plant Physiol.*, **152**, 151–165.
23. Wang,D., Xu,H., Huang,J.Y., Kong,Y.Z., AbuQamar,S., Yu,D.Q., Liu,S.Y., Zhou,G.K. and Chai,G.H. (2020) The Arabidopsis CCCH protein C3H14 contributes to basal defense against Botrytis cinerea mainly through the WRKY33-dependent pathway. *Plant Cell Environ.*, **43**, 1792–1806.
24. Wang,L., Xu,Y.Y., Zhang,C., Ma,Q.B., Joo,S.H., Kim,S.K., Xu,Z.H. and Chong,K. (2008) OsLIC, a novel CCCH-Type zinc finger protein with transcription activation, mediates rice architecture via brassinosteroids signaling. *PLoS ONE*, **3**, e3521.
25. Zhai,K.R., Deng,Y.W., Liang,D., Tang,J., Liu,J., Yan,B.X., Yin,X., Lin,H., Chen,F.D., Yang,D.Y. *et al.* (2019) RRM transcription factors interact with NLRs and regulate broad-spectrum blast resistance in rice. *Mol. Cell*, **74**, 996–1009.
26. Wang,R.Y., Ning,Y.S., Shi,X.T., He,F., Zhang,C.Y., Fan,J.B., Jiang,N., Zhang,Y., Zhang,T., Hu,Y.J. *et al.* (2016) Immunity to rice blast disease by suppression of effector-triggered necrosis. *Curr. Biol.*, **26**, 2399–2411.
27. Zhang,C.Y., Fang,H., Shi,X.T., He,F., Wang,R.Y., Fan,J.B., Bai,P.F., Wang,J.Y., Park,C.H., Bellizzi,M. *et al.* (2020) A fungal effector and a rice NLR protein have antagonistic effects on a Bowman-Birk trypsin inhibitor. *Plant Biotechnol. J.*, **18**, 2354–2363.
28. Lee,H.J., Park,Y.J., Seo,P.J., Kim,J.H., Sim,H.J., Kim,S.G. and Park,C.M. (2015) Systemic immunity requires SnRK2.8-Mediated nuclear import of NPR1 in Arabidopsis. *Plant Cell*, **27**, 3425–3438.
29. Fang,H., Shen,S.Q., Wang,D., Zhang,F., Zhang,C.Y., Wang,Z.X., Zhou,Q.Q., Wang,R.Y., Tao,H., He,F. *et al.* (2021) A monocot-specific hydroxycinnamoylputrescine gene cluster contributes to immunity and cell death in rice. *Sci. Bull.*, **66**, 2381–2393.
30. Li,W.T., Zhu,Z.W., Chern,M., Yin,J.J., Yang,C., Ran,L., Cheng,M.P., He,M., Wang,K., Wang,J. *et al.* (2017) A natural allele of a transcription factor in rice confers broad-spectrum blast resistance. *Cell*, **170**, 114–126.
31. Kawahara,Y., de la Bastide,M., Hamilton,J.P., Kanamori,H., McCombie,W.R., Ouyang,S., Schwartz,D.C., Tanaka,T., Wu,J.Z., Zhou,S.G. *et al.* (2013) Improvemenet of the *Oryza sativa* Nipponbare reference genome using next generation sequence and optical map data. *Rice*, **6**, 4.
32. Langmead,B. and Salzberg,S.L. (2012) Fast gapped-read alignment with Bowtie 2. *Nat. Methods*, **9**, 357–359.
33. Yu,G.C., Wang,L.G. and He,Q.Y. (2015) ChIPseeker: an R/Bioconductor package for ChIP peak annotation, comparison and visualization. *Bioinformatics*, **31**, 2382–2383.
34. Zhang,Y., Liu,T., Meyer,C.A., Eeckhoute,J., Johnson,D.S., Bernstein,B.E., Nussbaum,C., Myers,R.M., Brown,M., Li,W. *et al.* (2008) Model-based analysis of ChIP-Seq (MACS). *Genome Biol.*, **9**, R137.
35. Bailey,T.L., Boden,M., Buske,F.A., Frith,M., Grant,C.E., Clementi,L., Ren,J.Y., Li,W.W. and Noble,W.S. (2009) MEME SUITE: tools for motif discovery and searching. *Nucleic Acids Res.*, **37**, W202–W208.
36. Zhou,X.G., Liao,H.C., Chern,M., Yin,J.J., Chen,Y.F., Wang,J.P., Zhu,X.B., Chen,Z.X., Yuan,C., Zhao,W. *et al.* (2018) Loss of function of a rice TPR-domain RNA-binding protein confers broad-spectrum disease resistance. *Proc. Natl. Acad. Sci. U.S.A.*, **115**, 3174–3179.
37. He,J., Liu,Y.Q., Yuan,D.Y., Duan,M.J., Liu,Y.L., Shen,Z.J., Yang,C.Y., Qiu,Z.Y., Liu,D.M., Wen,P.Z. *et al.* (2020) An R2R3 MYB transcription factor confers brown planthopper resistance by regulating the phenylalanine ammonia-lyase pathway in rice. *Proc. Natl. Acad. Sci. U.S.A.*, **117**, 271–277.
38. Fukushima,R.S. and Hatfield,R.D. (2001) Extraction and isolation of lignin for utilization as a standard to determine lignin concentration

using the acetyl bromide spectrophotometric method. *J. Agric. Food Chem.*, **49**, 3133–3139.
39. Shi,X.T., Long,Y., He,F., Zhang,C.Y., Wang,R.Y., Zhang,T., Wu,W., Hao,Z.Y., Wang,Y., Wang,G.L. *et al.* (2018) The fungal pathogen *Magnaporthe oryzae* suppresses innate immunity by modulating a host potassium channel. *PLoS Pathog.*, **14**, e1006878.
40. Hu,K.M., Cao,J.B., Zhang,J., Xia,F., Ke,Y.G., Zhang,H.T., Xie,W.Y., Liu,H.B., Cui,Y., Cao,Y.L. *et al.* (2017) Improvement of multiple agronomic traits by a disease resistance gene via cell wall reinforcement. *Nat. Plants*, **3**, 17009.
41. Malukani,K.K., Ranjan,A., Hota,S.J., Patel,H.K. and Sonti,R.V. (2020) Dual activities of receptor-like kinase OsWAKL21.2 induce immune responses. *Plant Physiol.*, **183**, 1345–1363.
42. Li,W.T., Wang,K., Chern,M., Liu,Y.C., Zhu,Z.W., Liu,J., Zhu,X.B., Yin,J.J., Ran,L., Xiong,J. *et al.* (2020) Sclerenchyma cell thickening through enhanced lignification induced by OsMYB30 prevents fungal penetration of rice leaves. *New Phytol*, **226**, 1850–1863.
43. Bathe,U. and Tissier,A. (2019) Cytochrome P450 enzymes: a driving force of plant diterpene diversity. *Phytochemistry*, **161**, 149–162.
44. Mizutani,M. and Sato,F. (2011) Unusual P450 reactions in plant secondary metabolism. *Arch. Biochem. Biophys.*, **507**, 194–203.
45. Nelson,D. and Werck-Reichhart,D. (2011) A P450-centric view of plant evolution. *Plant J.*, **66**, 194–211.
46. Hamberger,B. and Bak,S. (2013) Plant P450s as versatile drivers for evolution of species-specific chemical diversity. *Philos. Trans. R. Soc. Lond., B, Biol. Sci.*, **368**, 20120426.
47. Jacoby,R.P., Li,L., Huang,S.B., Pong Lee,C., Millar,A.H. and Taylor,N.L. (2012) Mitochondrial composition, function and stress response in plants. *J. Integr. Plant Biol.*, **54**, 887–906.
48. Timon-Gomez,A., Nyvltova,E., Abriata,L.A., Vila,A.J., Hosler,J. and Barrientos,A. (2018) Mitochondrial cytochrome *c* oxidase biogenesis: recent developments. *Semin. Cell Dev. Biol.*, **76**, 163–178.
49. Mizutani,M. and Ohta,D. (2010) Diversification of P450 genes during land plant evolution. *Annu. Rev. Plant Biol.*, **61**, 291–315.
50. Li,F.F. and Wang,A.M. (2018) RNA decay is an antiviral defense in plants that is counteracted by viral RNA silencing suppressors. *PLoS Pathog.*, **14**, e1007228.
51. Xu,J., Yang,J.Y., Niu,Q.W. and Chua,N.H. (2006) Arabidopsis DCP2, DCP1, and VARICOSE form a decapping complex required for postembryonic development. *Plant Cell*, **18**, 3386–3398.
52. Jan,A., Maruyama,K., Todaka,D., Kidokoro,S., Abo,M., Yoshimura,E., Shinozaki,K., Nakashima,K. and Yamaguchi-Shinozaki,K. (2013) OsTZF1, a CCCH-Tandem zinc finger protein, confers delayed senescence and stress tolerance in rice by regulating stress-related genes. *Plant Physiol.*, **161**, 1202–1216.
53. Wang,L.J., Pei,Z.Y., Tian,Y.C. and He,C.Z. (2005) OsLSD1, a rice zinc finger protein, regulates programmed cell death and callus differentiation. *Mol. Plant Microbe Interact.*, **18**, 375–384.
54. Liu,J.L., Park,C.H., He,F., Nagano,M., Wang,M., Bellizzi,M., Zhang,K., Zeng,X.S., Liu,W.D., Ning,Y.S. *et al.* (2015) The RhoGAP SPIN6 associates with SPL11 and OsRac1 and negatively regulates programmed cell death and innate immunity in rice. *PLoS Pathog.*, **11**, e1004629.
55. Wong,H.L., Pinontoan,R., Hayashi,K., Tabata,R., Yaeno,T., Hasegawa,K., Kojima,C., Yoshioka,H., Iba,K., Kawasaki,T. *et al.* (2007) Regulation of rice NADPH oxidase by binding of Rac GTPase to its N-terminal extension. *Plant Cell*, **19**, 4022–4034.
56. Amsbury,S. (2020) Sensing attack: the role of wall-associated kinases in plant pathogen responses. *Plant Physiol.*, **183**, 1420–1421.
57. Kohorn,B.D. and Kohorn,S.L. (2012) The cell wall-associated kinases, WAKs, as pectin receptors. *Front. Plant Sci.*, **3**, 88.
58. Wang,P., Zhou,L., Jamieson,P., Zhang,L., Zhao,Z.X., Babilonia,K., Shao,W.Y., Wu,L.Z., Mustafa,R., Amin,I. *et al.* (2020) The cotton wall-associated kinase GhWAK7A mediates responses to fungal wilt pathogens by complexing with the chitin sensory receptors. *Plant Cell*, **32**, 3978–4001.
59. Zhang,N., Pombo,M.A., Rosli,H.G. and Martin,G.B. (2020) Tomato wall-associated kinase SlWak1 depends on Fls2/Fls3 to promote apoplastic immune responses to *Pseudomonas syringae*. *Plant Physiol.*, **183**, 1869–1882.
60. Liu,B., Li,J.F., Ao,Y., Qu,J.W., Li,Z.Q., Su,J.B., Zhang,Y., Liu,J., Feng,D.R., Qi,K.B. *et al.* (2012) Lysin motif-containing proteins LYP4 and LYP6 play dual roles in peptidoglycan and chitin perception in rice innate immunity. *Plant Cell*, **24**, 3406–3419.
61. Shimizu,T., Nakano,T., Takamizawa,D., Desaki,Y., Ishii-Minami,N., Nishizawa,Y., Minami,E., Okada,K., Yamane,H., Kaku,H. *et al.* (2010) Two LysM receptor molecules, CEBiP and OsCERK1, cooperatively regulate chitin elicitor signaling in rice. *Plant J.*, **64**, 204–214.
62. Gunupuru,L.R., Arunachalam,C., Malla,K.B., Kahla,A., Perochon,A., Jia,J.G., Thapa,G. and Doohan,F.M. (2018) A wheat cytochrome P450 enhances both resistance to deoxynivalenol and grain yield. *PLos One*, **13**, e0204992.
63. Liu,Q., Khakimov,B., Cardenas,P.D., Cozzi,F., Olsen,C.E., Jensen,K.R., Hauser,T.P. and Bak,S. (2019) The cytochrome P450 CYP72A552 is key to production of hederagenin-based saponins that mediate plant defense against herbivores. *New Phytol.*, **222**, 1599–1609.
64. Irmler,S., Schroder,G., St-Pierre,B., Crouch,N.P., Hotze,M., Schmidt,J., Strack,D., Matern,U. and Schroder,J. (2000) Indole alkaloid biosynthesis in Catharanthus roseus: new enzyme activities and identification of cytochrome P450 CYP72A1 as secologanin synthase. *Plant J.*, **24**, 797–804.
65. Wang,Y.L., Li,Q. and He,Z.H. (2004) Blast fungus-induction and developmental and tissue-specific expression of a rice P450 CYP72A gene cluster. *Chinese Sci. Bull.*, **49**, 131–135.
66. Fedoroff,N.V. (2002) RNA-binding proteins in plants: the tip of an iceberg? *Curr. Opin. Plant Biol.*, **5**, 452–459.
67. Maldonado-Bonilla,L.D., Eschen-Lippold,L., Gago-Zachert,S., Tabassum,N., Bauer,N., Scheel,D. and Lee,J. (2014) The Arabidopsis tandem zinc finger 9 protein binds RNA and mediates pathogen-associated molecular pattern-triggered immune responses. *Plant Cell Physiol.*, **55**, 412–425.
68. Li,Y.S., Chen,L.C., Mu,J.Y. and Zuo,J.R. (2013) LESION SIMULATING DISEASE1 interacts with catalases to regulate hypersensitive cell death in Arabidopsis. *Plant Physiol.*, **163**, 1059–1070.
69. Kawano,Y., Akamatsu,A., Hayashi,K., Housen,Y., Okuda,J., Yao,A., Nakashima,A., Takahashi,H., Yoshida,H., Wong,H.L. *et al.* (2010) Activation of a Rac GTPase by the NLR family disease resistance protein Pit plays a critical role in rice innate immunity. *Cell Host Microbe*, **7**, 362–375.
70. Akamatsu,A., Wong,H.L., Fujiwara,M., Okuda,J., Nishide,K., Uno,K., Imai,K., Umemura,K., Kawasaki,T., Kawano,Y. *et al.* (2013) An OsCEBiP/OsCERK1-OsRacGEF1-OsRac1 module is an essential early component of chitin-induced rice immunity. *Cell Host Microbe*, **13**, 465–476.
71. Kawasaki,T., Henmi,K., Ono,E., Hatakeyama,S., Iwano,M., Satoh,H. and Shimamoto,K. (1999) The small GTP-binding protein Rac is a regulator of cell death in plants. *Proc. Natl. Acad. Sci. U.S.A.*, **96**, 10922–10926.